2016-07-11

Brain Tissue Responses to Utah Microelectrode Arrays

Anette I. Pico
University of Miami, pico.anette@gmail.com

UNIVERSITY OF MIAMI

BRAIN TISSUE RESPONSES TO UTAH MICROELECTRODE ARRAYS

By

Anette I. Pico

A THESIS

Submitted to the Faculty
of the University of Miami
in partial fulfillment of the requirements for
the degree of Master of Science

Coral Gables, Florida

August 2016

UNIVERSITY OF MIAMI

A thesis submitted in partial fulfillment of
the requirements for the degree of
Master of Science

BRAIN TISSUE RESPONSES TO UTAH MICROELECTRODE ARRAYS

Anette I. Pico

Approved:

_____ Abhishek Prasad, Ph.D. Assistant Professor of Biomedical Engineering	_____ Suhrud M. Rajguru, Ph.D. Assistant Professor of Biomedical Engineering and Otolaryngology
_____ Esperanza Bas Infante, PharmD, Ph.D. Research Assistant Professor of Otolaryngology	_____ Guillermo J. Prado, Ph.D. Dean of the Graduate School

PICO, ANETTE I. (M.S., Biomedical Engineering)
Brain Tissue Responses to Utah Microelectrode Arrays. (August 2016)

Abstract of a thesis at the University of Miami.

Thesis supervised by Abhishek Prasad, Ph.D.
No. of pages in text. (76)

Microelectrode arrays have been widely used to record and analyze neural signals and activity aiding in the detection of brain injuries. The current techniques for electrode implantation involve invasive surgical procedures in which the electrode array is slowly inserted into the brain tissue. Implanted electrodes can be affected by both abiotic (insulation, metal, corrosion, etc.) and biotic (neuroinflammation, blood brain barrier damage, etc.) factors that lead to degradation of recorded signals during chronic time periods. In order to better understand the response to microelectrode implantation, the biotic factors that contribute to their eventual decay and further tissue deterioration have been characterized. The goal of this thesis is to understand the acute biotic processes that occur during the rapid insertion of Utah microelectrode arrays; we attempt to study, in detail, the neuroinflammatory response involved in neural electrode implants. We compare microglial, astroglial, and vascular disruption markers in short-term implanted animals to assess the effects of neuroinflammation from rapid insertion of Utah arrays. We also evaluate the expression of axonal biomarkers from serum and cerebrospinal fluid (CSF) in relation to electrode performance and neural injury.

Acknowledgments

I would like to express my deepest gratitude to my advisor, Dr. Abhishek Prasad, for his guidance, mentorship, and endless patience throughout this work. I would also like to thank Dr. Suhrud Rajguru and Dr. Esperanza Bas Infante for being a part of my committee and helping me complete my graduate degree. Many thanks go to Yee-Shuan for sharing her dry-ice and knowledge with me and to Dr. Agarwal's lab for allowing us to use their equipment. This work could not have been accomplished without Farrah Mohammed; thank you for your infinite help and companionship throughout this entire project.

A special thank you goes to Zoltan Buchwald for his unconditional love and support in all things. Lastly, I would like to thank my parents and brother for their continuous encouragement and affection.

TABLE OF CONTENTS

Page

LIST OF FIGURES ..... **vi**

LIST OF TABLES ..... **viii**

Chapter 1: Introduction and Goals **1**

Chapter 2: Background **4**

2.1 Microelectrodes 4

2.1.1 The Utah Array 4

2.1.2 Electrode Performance and Deterioration 5

2.2 General Anatomy and Physiology 7

2.2.1 The Nervous System 7

2.2.2 Neurons 8

2.2.3 Glial Cells 10

2.3 Injury Response 11

2.4 Chronic injury biomarkers 15

2.4.1 Phosphorylated Axonal Neurofilament Subunit (pNF-H) 15

2.4.2 Ubiquitin C-Terminal Hydrolase 1 (UCHL1) 17

2.5 Histology and Immunohistochemistry 18

2.5.1 Antigens and Antibodies 18

2.5.2 Immunohistochemical Markers for Neuroinflammation 20

2.6 Significance 22

Chapter 3: Materials and Methods **23**

3.1 Experimental Design 23

3.2 Microelectrode Implant Surgery 24

3.3 Blood collection …..... 28

3.4 Perfusion 29

3.5 ELISA 30

3.6 Tissue Embedding 31

3.7 Freezing and Cryosectioning 33
3.8 Immunostaining 36
3.8.1 Day 1: Primary Antibodies 36
3.8.2 Day 2: Secondary Antibodies 37
3.9 Histopathology 38
3.10 Analysis 39

Chapter 4: Results and Discussion 40
4.1 Markers of Injury 40
4.1.1 Biochemical Analysis of Acute Implants 40
4.1.2 Temporal Evolution 43
4.1.3 Coupling Functional and Biochemical Factors 44
4.2 Immunohistochemistry 46
4.2.1 Two- and Four-Week Stab Animals 50
4.2.2 Two-Week Stab and Four-Week Implant Animals 52
4.2.3 Four-Week Stab and Implant Animals 54
4.3 Supplementary Data 56
4.3.1 Two-Week Stab Animals 56
4.3.2 Four-Week Stab Animals 60
4.3.3 Four-Week Implant Animals 64

Chapter 5: Conclusion 68
5.1 Summary …..... 68
5.2 Limitations 69
REFERENCES 70

LIST OF FIGURES

Figure Page

Figure 2.1 4

Figure 2.2 7

Figure 2.3 8

Figure 2.4 12

Figure 2.5 19

Figure 3.1 25

Figure 3.2 27

Figure 3.3 32

Figure 3.4 35

Figure 3.5 39

Figure 4.1 41

Figure 4.2 42

Figure 4.3 43

Figure 4.4 45

Figure 4.5 50

Figure 4.6 50

Figure 4.7 51

Figure 4.8 51

Figure 4.9 52

Figure 4.10 52

Figure 4.11 53

Figure 4.12 53
Figure 4.13 54
Figure 4.14 54
Figure 4.15 55
Figure 4.16 55
Figure 4.17 56
Figure 4.18 57
Figure 4.19 58
Figure 4.20 59
Figure 4.21 60
Figure 4.22 61
Figure 4.23 62
Figure 4.24 63
Figure 4.25 64
Figure 4.26 65
Figure 4.27 66
Figure 4.28 67

LIST OF TABLES

Table Page

Table 3.1 39

Chapter 1: Introduction and Goals

Brain injuries can arise from multifaceted neural diseases and disorders that compromise the livelihood and functionality of neurons and tissue. Neural impairment has previously been targeted with neural prosthetic devices that can be used to restore communication and control after an injury to the nervous system. Neuroprosthetic devices rely on microelectrode arrays to record neuronal activity (Biran et al., 2005, Lacour et al., 2010, Mccreery et al., 1997, Nicolelis et al., 2002, Polikov et al., 2005). Electrodes in the neural tissue are affected by both abiotic (insulation, metal, corrosion, etc.) and biotic (neuroinflammation, blood brain barrier damage, etc.) factors which lead to degradation in the recorded signal during chronic time periods. An interplay of these factors leads to temporal degradation of recorded signals in the chronic period ultimately resulting in electrode failure, in which the electrode is unable to isolate single action potentials. In order to better understand the response to microelectrode implantation, the biotic and abiotic factors that contribute to their eventual decay and further tissue deterioration have been characterized and improved to obtain superior function in a given environment (Geddes and Roeder 2003, Prasad et al., 2011, Prasad et al., 2012, Turner et al., 1999). Electrode failure is a complex, dynamic, multi-faceted problem where each of these factors occurs at varying time-scales. In this thesis, we attempt to study in detail one of the biotic factors involved in neural electrode implants. In this study, we compare the astroglial, microglial, and markers for vascular disruption in short-term animals implanted with Utah microelectrode arrays. We also compare biomarkers of injury as obtained from serum or cerebrospinal fluid and assess their expression.

Neural injury biomarkers can be easily monitored from blood as a novel technique

for detecting brain injuries. Although previous studies have backed the reliability of neural markers as potential sources for diagnoses of brain damage, much of the data and the types of injuries they can be utilized to detect it remain unclear. Previous focus on two neuronal injury biomarkers known as the phosphorylated axonal neurofilament subunit (pNF-H) and ubiquitin C-terminal hydrolase 1 (UCHL1), have provided support of their potential as novel indicators of acute brain injury (Lewis et al., 2008, Lewis et al., 2010, Shaw et al., 2005, Siman et al., 2008). One study, solely focused on the detectability of pNF-H, finds that the upregulation of such a marker constitutes neural damage consistent with spinal cord and traumatic brain injury (Shaw et al., 2005). Another published study paid attention to UCHL1 expression patterns complementing neuronal cell loss in patients and attributed the biomarker as a potential indicator of brain injury and deterioration (Lewis et al., 2010). Nonetheless, research surrounding the variation of these markers has not been sufficiently associated with microelectrode-induced injuries to attest their validity as prominent prognosticators of neural damage. Instead, most studies only observe the neuronal changes from histology assessments that can only be performed on extracted tissue.

Biran et al., (2005) recorded the inflammatory response that occurs after brain injury caused by implanted silicon microelectrode arrays. They showed the damage to the brain tissue as a result of microelectrode implantation in a cohort of animals (Biran et al., 2005). Other studies have also recorded the tissue responses as a cause of implanted electrode arrays and shown that reactive gliosis is a major contributor of neuroinflammation (Fernández et al., 2014, Polikov et al., 2005, Prasad et al., 2012, Szarowski et al., 2003, Winslow and Tresco 2010). The above mentioned literature provides promising results for both the analysis of cellular responses as cues of neural

injury and the progressing neuroinflammatory and encapsulation cascade caused by implanted electrode microarrays. Much like Biran et al. (2005) tested silicon arrays in stab wound and acute implants, our approach will focus on the cross-examination of BBB (blood-brain barrier) damage and reactive gliosis in Utah microelectrode-induced stab wound and acute-term implants to better understand injury caused by insertion of these electrodes.

The goal of this thesis is to understand the acute biotic processes that occur during the rapid insertion of Utah microelectrode arrays. This was accomplished by performing a routine craniotomy in male, adult Sprague-Dawley rats and rapidly inserting the microelectrode into the somatosensory cortex of each animal. The array was then either carefully removed or left in place for the remainder of the experiment. The brain tissue of each animal was examined with immunohistochemical markers of neuroinflammation as indicators of the penetrating injury created by the microelectrode implant surgery. This experimental setup was chosen to compare implanted and stabbed cohorts, thus allowing singular and collective assessments of histological markers that, if similar, make the insertion effects of these electrodes a contributing factor to the neuroinflammatory response.

Chapter 2: Background

2.1 Microelectrodes

2.1.1 The Utah Array

Microelectrode arrays have been important tools in furthering knowledge of neural activity and function. Method for studying nerve cells and their interactions in the nervous system utilize electrical stimulation and signal recording for the assessment of neural activity (Maynard et al., 1997, Mccreery et al., 1997, Nicolelis and Ribeiro 2002). Like other electrodes, Utah electrode arrays (UEA) have been used as neuroprosthetic tools to electrically stimulate or record activity of neurons (Rousche and Normann 1998, Rousche and Normann 1992).

The UEA is assembled from a silicon block that, through etching, doping, and heat treatment, results in a matrix with electrode shanks and recording tips (Polikov et al., 2005). The microarray is a square-shaped, silicon substrate structure that can be situated into the neural cortex and used in cortical applications as a rehabilitative prosthetic device in the

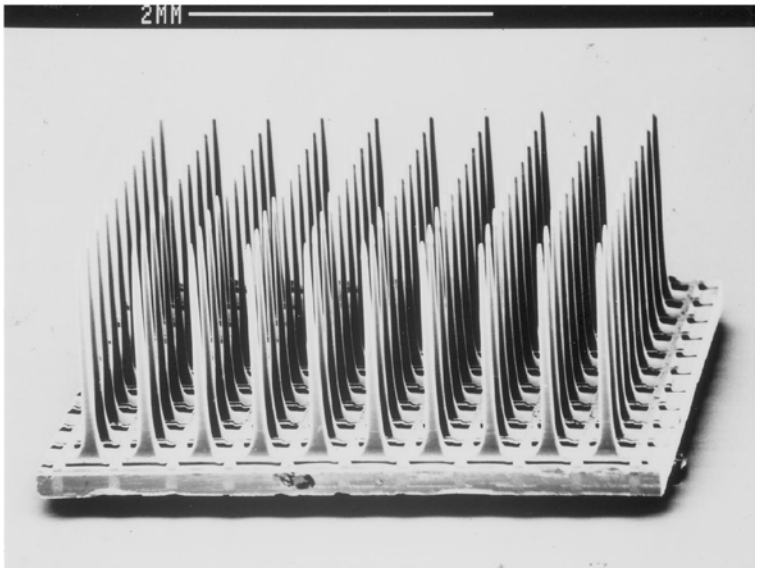

Figure 2.1: Standard Utah Electrode Array constructed from a single silicon block (Rousche & Normann 1998).

brain. These arrays tend to be standardly constructed as 10 x 10 matrices comprised of 100 electrode shanks with 400μm of separation between each shank, where each shank is 1.5mm in length (Nordhausen et al., 1994). The electrodes we focus on, however, are custom built as 4 x 4 matrices containing a total of 16 shanks with the same set of properties as the standards. The shafts are insulated with parylene-C and the units are 80μm thick at the base and then taper into a fine metalized tip. Although many of these arrays are used to record neural activity, we focus on the use of nonfunctional arrays as a means to temporally and spatially observe the tissue response to injury via histological techniques.

2.1.2 Electrode Performance and Deterioration

The performance of electrode arrays depends on different biotic and abiotic factors that can interfere with the microarray and vice versa. Poor electrode performance and failure can be attributed to mechanical, material, and biological factors pertaining to the device and the surrounding tissue in which the array is embedded (Prasad et al., 2011, Prasad et al., 2014, Prasad and Sanchez 2012). Since the Utah arrays we utilize are implanted as non-recording devices, electrode performance and the features diminishing functionality are not explored in detail. Instead, factors that affect electrode degradation and, by consequence, surrounding neural tissue, are of main concern in further investigating the insertion effects of implanting microelectrode arrays in the somatosensory cortex. It is important to note, however, that electrode performance can also contribute to neuroinflammation and the foreign body response. The implanted electrode arrays are capable of damaging tissue at the implant site and cause environmental disruptions that result in disturbances to the BBB, cell recruitment, and neuron death (Biran et al., 2005, Fernández et al., 2014).

Here, we focus on animals surviving up to 28 days with an implant, a period of time in which the neural tissue expresses distinct cues as a result of foreign materials. For instance, local neurodegeneration as a result of neuronal and glial cell loss that can be promoted by chronic electrode injury may be expressed in implanted animals four-weeks post-surgery (McConnell et al., 2009). Biological degradation occurring after an electrode implant results in further damage and deterioration of the living tissue around the implanted array as a result of the inflammatory response (Biran et al., 2005, Fernández et al., 2014). Other studies have demonstrated that electrode performance and deterioration is unaffected by neuroinflammatory patterns, including but not limited to recording electrodes where the functionality of the recording site has been unaffected (Freire et al., 2011). To explain, in functional, recording arrays, electrode performance tends to vary from poor, where neuron recordings are low, to good, where recordings and electrode performance are high, despite the severity of inflammation present. According to Kozai et al. (2015) performance and degradation variability are a combination of material and biological failures, such that it cannot all be attributed to the inflammatory response. The neural tissue is prone to decay by biological responses as a result of neurodegeneration and neuroinflammation caused by injury from the electrode arrays. The arrays, however, may also decay from longevity inside the tissue. Several failure modes that can occur to the arrays include corrosion, cracking, bending of the electrode shanks, and delamination or cracking of the parylene-C insulation (Kozai et al., 2015). These factors, alongside tissue reactions, contribute to the damage by the implanted device to the surrounding tissue.

2.2 General Anatomy and Physiology

2.2.1 The Nervous System

The body's nervous system is composed of both the central and peripheral nervous systems. The central nervous system (CNS) is comprised of the spinal cord and brain, while the peripheral nervous system (PNS) constitutes all other parts of the nervous system, such as the spinal nerves. More importantly, we focus on the neural damage that occurs when the somatosensory cortex is injured in rat brains. The somatosensory cortex, located on the parietal lobe behind the central sulcus, processes somatosensory stimuli that when electrically stimulated may provoke sensations (Bear at al., 2007). This part of the cerebral cortex is highly sensitive and receives dense amounts of input that are processed by slow and fast adapting nerve cells contained in the area. Furthermore, since the brain is a highly protected organ encased in different strata, in order to access the somatosensory cortex in the brain, several layers of bone and muscle cells have to be removed. Among these, are the skin, periosteum, skull, and meninges which are layers of connective tissue that isolate

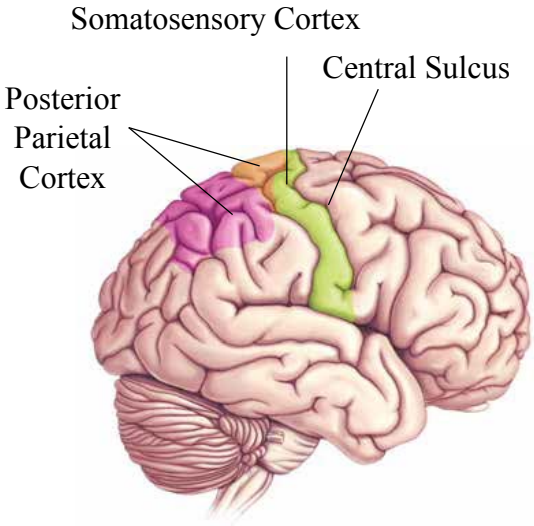

Figure 2.2: The exact position of the somatosensory cortex behind the central sulcus on the parietal lobe (Bear et al., 2007).

the brain inside the skull. Once these layers are removed, and the somatosensory cortex is exposed, injury may be triggered by stabbing the brain tissue, thereby disrupting the blood-brain barrier (BBB) and activating neuronal and glial cell responses.

2.2.2 Neurons

A neuron, otherwise known as a nerve cell, is specialized to transmit, receive, and store information through electrochemical signals. These cells are hardwired to communicate responses and emit processes such as protein synthesis and energy production (Bear et al., 2007). The simplified structure of a neuron consists of a neuronal membrane, the soma or cell body, the axon, and the dendrites. Unlike neurons, glial cells don't possess axons or dendrites, regarding neurons as specialized cells that can emit electrical impulses. To explain, the soma or cell body of a neuron contains the common

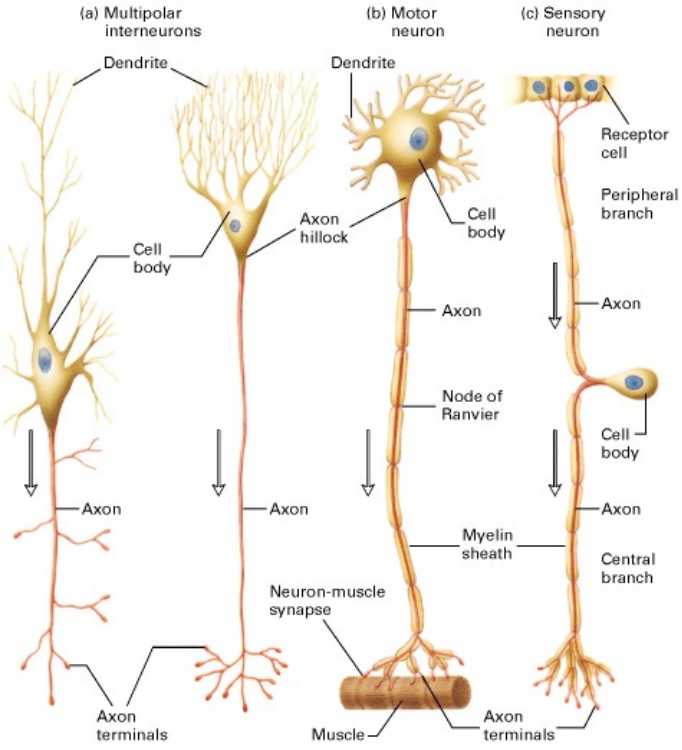

Figure 2.3: Structures of neurons. (a) Multipolar interneurons. (b) Motor neuron. (c) Sensory neuron (Lodish et al., 2000).

organelles found in all cells, such as the nucleus, mitochondria, and the Golgi apparatus, among others. The cell body is the site where most protein synthesis and assembling occurs (Lodish et al., 2000). After, all of the constructed neuronal proteins and membranes are transferred down the length of the axon towards the axon terminal, this occurs by a process known as anterograde transport.

The axon, as seen in figure 2.3, is a unique part of neurons through where electrical impulses known as action potentials are run down to transmit signals to nearby nerve cells. Unlike the cell body of a neuron, the axon is distinctly used for the transfer of action potentials. The point of signal transfer, known as the synapse, is usually where one nerve cell innervates other cells upon interaction. Once synaptic transmission has been achieved, surrounding neurons receive the electrical signals through their multitude of dendrites, which extend outward from the soma. Dendrites, another structure unique to nerve cells, are able to transport incoming signals into the soma as small electrical impulses (Lodish et al., 2000). Although there is more detail in how neurons emit and receive action potentials, this simplified version on how nerve cells operate provides insight into their complex functional aspects.

Furthermore, as noted in figure 2.3, there are three classes of neurons, motor neurons that control voluntary muscle movement, sensory neurons which carry information from sensory organs to the brain, and interneurons that are in charge of forming connections between other neurons (Bear et al., 2007). It is important to note that all information received by the brain, permitting day-to-day activities is processed by nerve cells and the intricate network of connections they form in our nervous systems. As such, when nerve cells are damaged and die there is a deficiency of signals being transmitted and

expressed, resulting in distinct life-altering consequences; the loss of cognitive skills, memory, muscle control, and paralysis are just a few of the possible effects of deceased or degenerated neurons.

2.2.3 Glial Cells

Non-neuronal cells that provide support for nerve cells in the central and peripheral nervous systems are known as glial cells. Although these cells are not known for emitting electrical stimulation, they are in charge of insulating, supporting, and nourishing surrounding neurons; glial cells provide a framework for nerve cells to function and are involved in processes such as the immune response (Bear et al., 2007). Amongst non-neuronal cells, each different type of glia individually contributes to the function of the nervous system. For example, one of the most abundant glial cells in the brain, astrocytes, seal most of the gaps between nerve cells, affecting the potential growth of neurons. One of the main functions of astrocytes is the chemical regulation of the neuronal synapses; astrocytes exert this chemical balance, for instance, by limiting the number of neurotransmitters that are released into the extracellular space. Another important function of astrocytes is the concentration control of substances that could interfere with neurons and their processes (Bear at al., 2007). In addition, other types of glia, such as oligodendrocytes and Schwann cells, which can be found in the peripheral nervous system, are called myelinating glia as their main task is to provide layers of myelin sheath used to insulate the axons of nerve cells.

Microglia are cells that function as phagocytic cells in the removal of dead or degenerating neuronal and non-neuronal cells (Graeber and Streit 2009, Vihardt 2005). In recent studies, these cells have shown migration patterns from the blood into the brain, a

process that if interrupted can alter neural function (Bear et al., 2007, Fernández et al., 2014). Experimental interpretations of these cells have also indicated that microglial activation is a factor of present and ongoing neural damage and degeneration (Block et al., 2007, Graeber and Streit 2009, Vihardt 2005). Reactive gliosis, which contributes to the migration of microglia and macrophages to a site of injury has shown to contribute to neuron death (Biran et al., 2005).

2.3 Injury Response

Implanting materials into the body is associated with different immune reactions, such as the inflammatory, wound healing, and foreign body response. During a surgical implant, specifically that of a microelectrode into the brain tissue, the body elicits a cascade of immune reactions as a result to injury. First, understanding the concept of biocompatibility when working with implants is vital to developing knowledge of the inflammatory and injury responses. Biocompatibility can be better defined as the coexistence of host tissue with a foreign material and their concurrence to provoke systemic responses in the implanted body. The body's reaction to foreign materials is imperative as it can directly affect the safety or biocompatibility of a medical device, prosthesis, or implanted biomaterial as well as the short- and long-term tissue response (Anderson et al., 2008, Williams et al., 1999, Winslow and Tresco 2010). In other words, the biocompatibility of an implant does not only affect the host tissue, but the reactive responses that occur as a result of the procedure can itself contribute to device failure and degradation. The body's innate inflammatory response occurs in various stages as a means to initiate the healing process at the site of injury. Cellular activation as a result of injury is one of the recruiting factors for the inflammatory response to commence (Rock et al.,

2008). However, since the focus of this manuscript lies in neural injury, we will be concentrating on neuroinflammatory patterns, rather than the whole body's inflammation cascade. In turn, this will allow us to specifically understand the healing stages that occur in neural tissue after a microelectrode implant. For instance, activated microglia cells secrete many pro-inflammatory factors that contribute to the neuroinflammatory process (Dahlke et al., 2015). Microglia, however, are not the only cells that promote the injury response. Neurological injury leads to the recruitment of other glial cells that contribute to the neuroinflammatory response that results from nerve cell damage as shown in Figure

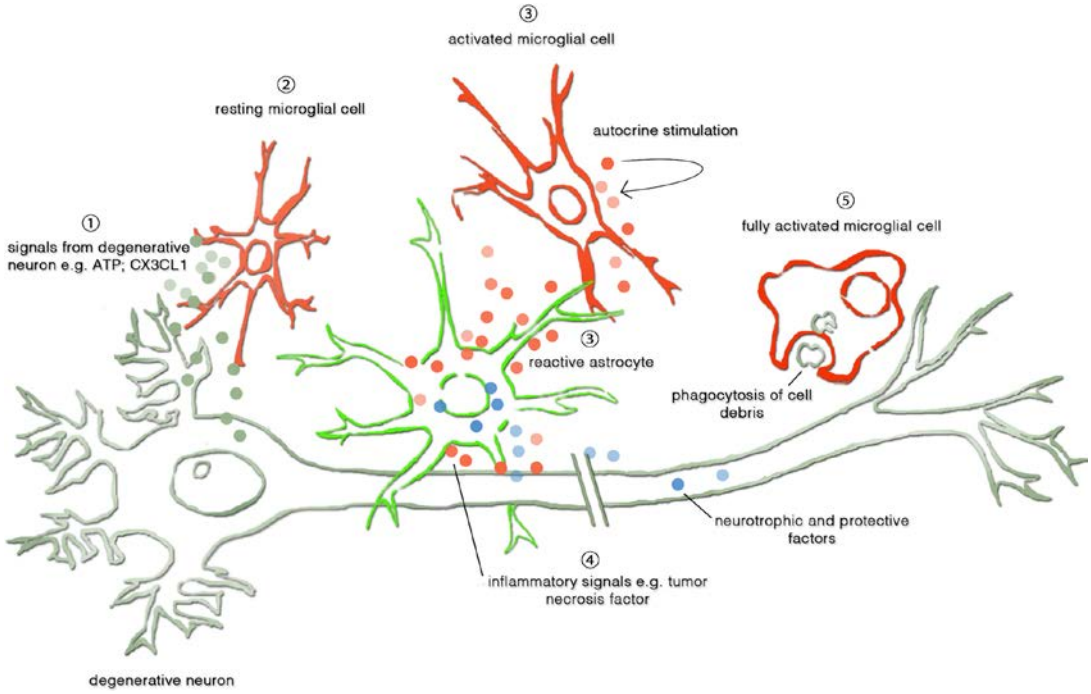

Figure 2.4: Minimalized diagram of the neuroinflammatory process occurring after neurons are injured (Dahlke et al., 2015).

2.4. Although we mainly assess the consequences of implanting neuroprosthetic devices, other types of neural injury convening from diseases such as Parkinson's, Alzheimer's, Huntington's, and ALS (amyotrophic lateral sclerosis) also lead to neuroinflammation and may elicit greater damage as their degree of injury tends to affect larger portions of the brain tissue. Muszynski et al. (2016) observes that neurological surgery and traumatic brain

injuries have the capacity to impair innate immune reactions and lead to secondary infection.

Furthermore, much like the process described by Lv et al. (2015) a neuroprosthetic implant causes primary injury by the initial perforation of tissue and physical contact between the host and the device. Consequently, after the initial injury is produced, a secondary injury reaction is triggered by distinct cellular and chemical pathways causing reactive cellular responses, neuronal inflammation, oxidative stress, and nerve cell degeneration and death (Lv et al, 2015). Following the secondary injury pathway, many of the inherent changes that occur in cell morphology and recruitment, as well as tissue response in the process of healing cannot be reversed. As such, if neuronal function or reactivity is lost during the neuroinflammatory process, they cannot be recuperated and result in additional damage caused by an innate immune response (Lv et al., 2015). This, then, becomes a primary concern of implantable neuroprosthetic devices. The probabilities of inducing further damage through implantation of a device and incapacitating or eradicating functional neurons and viable tissue results in hesitation of whether the benefits outweigh the potential detriments.

Moreover, cellular activation is a particularly important aftermath of neural injury. Chronic and acute neuronal degeneration and apoptosis has been studied in relation to cellular responsivity. As previously mentioned, neurological diseases that chronically affect the brain contribute to activation of microglial and astroglial cells as a response to nerve cell degeneration (Dahlke et al., 2015). In the case of neural damage through neuroprostheses, the injury procured thru a craniotomy and perforating tissue with an electrode has been heavily associated with chronic neurodegeneration and disruption of the

blood-brain barrier leading to neuroinflammation (Guy et al., 2008). The resulting activation of microglia and astrocytes provides insight of how cellular activation and the inflammatory process is related to nerve cell and tissue death or damage. A good approach to describing tissue response has been described by Szarowski et al. (2003), where it is explained how implanted neuroprosthetics are insulated by a cellular encapsulation sheath, thus isolating the device from the brain. In other words, histological analysis of implanted devices has validated a process known as reactive gliosis, in which a change in the central nervous system, in this case an injury, promotes responses in glial cells (Turner et al., 1999). On implanted neural devices, studies have noted increases in the expression and morphology of glial fibrillary acidic protein (GFAP) by astrocytes and microglia, which tend to form a cellular sheath around inserted silicon devices (Spataro et al., 2005, Szarowski et al., 2003). The encapsulation sheath by which many devices are isolated from the brain, although it diminishes the potential of the device as a therapeutic tool, offers insight into the volume and severity of the trauma as it is a sign of tissue damage from the initial puncture and may serve as a temporal cue for assessing neuroinflammation (Spataro et al., 2005, Szarowski et al., 2003). In turn, cellular activity and other factors surrounding and arising from neural injury are vital in understanding how the host tissue and a foreign device interact. As such, establishing an understanding of the neuroinflammatory process after an implant will be critical in assessing the degree of injury caused by implanting microelectrode arrays. The temporal patterns of factors contributing to the evaluation of injury, such as quantification of biomarkers and histological analyses will be considered in the progressing study of the neuroinflammatory response.

2.4 Chronic Injury Biomarkers

2.4.1. Phosphorylated Axonal Neurofilament Subunit (pNF-H)

The phosphorylated axonal neurofilament subunit (pNF-H) can be characterized as the heavily phosphorylated form of neurofilament subunit H. The neurofilament heavy protein subunit, NF-H, is one of three neuronal cytoskeleton intermediate filament subunit proteins, where the other two are neurofilament median and light protein (McCombe et al., 2015). Its phosphorylated constituent, pNF-H, has been found in the axons of large projecting neurons, which are nerve cells whose axons extend from the cell body to other distal areas in the central nervous system. The amino acid sequence of this protein is quite rare, as it contains regions of many repetitions of the amino acids lysine, serine, and proline, in that order. This uncommon peptide is only known in approximately 50 other mammalian NF-H protein sequences (Lee et al., 1988). The known phosphorylated form of NF-H that we focus on, contains all phosphorylated lysine, serine, and proline peptides in axonal neurofilaments. In other words, the neurofilaments of perikarya, dendrites, and proximal axons are not phosphorylated, yet the neuroflaments of long projecting neurons and their terminal axons are found to be highly phosphorylated, allowing the distinction between an NF-H unit and its heavily phosphorylated form, pNF-H (Sternberger L. & Sternberger N. 1983). This distinction, in turn, also provides evidence that pNF-H can be used as a reliable axonal marker; this marker is usually better represented in later stages of growth when it becomes phosphorylated, such that it may also be used as a marker for nerve cell development.

Moreover, because this protein is specific to neurons and their axons, pNF-H has been studied in relation to neurological diseases and disorders, as well as induced neural

injury that harms nerve cells and the brain tissue (Petzold 2005, Petzold and Shaw 2007). Detection of pNF-H through cerebrospinal fluid (CSF) and serum has been performed in subjects with distinct spinal cord and brain lesions, that could have occurred from a neurological disease, an incident affecting nerve cells, or a cardiac arrest and ischemic stroke eliciting acute brain injury (Hayakawa et al., 2012, Hu et al., 2002, McCombe et al., 2015, Ohya et al., 2015, Singh et al., 2011, Žurek et al., 2011). As a result of such promising scientific research, pNF-H has been promoted as a potentially reputable source of neuronal and axonal injury, deterioration, or degradation. Although CSF has been the more utilized fluid from which to obtain measureable readings of pNF-H, more present studies are deviating and utilizing sera as the primary source for detection. Several reasons are considered for the use of sera as the main method of detection, among which lie the obvious facts that it is an easier and more routine procedure that may also be used to detect spinal cord and brain lesions in animals (Mondello et al., 2011, Shaw et al., 2005). Furthermore, other factors that make pNF-H an exciting biomarker for detecting neural injury and damage include its abundancy as a component of axons. The copious presence of pNF-H in axons leads to the hypothesis of its release following damage; assuming that this protein is present in axons as studies continue to demonstrate, pNF-H should be released after axonal injury and be readily available in sera for detection with an ELISA kit (enzyme-linked immunosorbent assay) (Boylan et al., 2009, Ghonemi et al., 2013, Gresle et al., 2008, Matsushige et al., 2008). According to Pant (1988), the heavy phosphorylation of this protein makes it resilient to proteolysis, such that the protein remains viable in sera and CSF for an extended time period, making its detection easier. Also, the known immunogenicity of this protein in combination with the multi-epitope composition of the

phosphorylated filaments make it abundant in the process of detection. As previously mentioned, this subunit is released and available as a reflection of axonal injury and different disorders and diseases that either result from or provoke axonal injury (Stys 2005). Lastly, since pNF-H has been characterized as a degenerative marker and its upregulation has been associated to the degree of axonal injury present in nerve cells, we utilize this biomarker as a source of progressing neuroinflammation and injury after an electrode implant.

2.4.2 Ubiquitin C-Terminal Hydrolase 1 (UCHL1)

Ubiquitin C-terminal hydrolase 1 (UCHL1) otherwise known as neuron specific protein PGP 9.5, ubiquitin carboxyl esterase L1, ubiquitin thiolesterase, or Park5 is a proteolytically stable protein found in nerve cells (Wilkinson et al., 1989). Although now widely known as UCHL1 due to its enzymatic activity, this protein was originally designated the name PGP 9.5 after its detection in the neuronal cytoplasm of a 2-dimensional gel analysis (Doran et al., 1983). Through its discovery, UCHL1 was observed in abundance in the brain where its estimated presence amounted to concentrations of 200-500 μg/g wet weight, or approximately 1-2% of total brain protein, comprising it as a major constituent of neuronal cytoplasm (Doran et al., 1983).

Moreover, among its various functions and roles, UCHL1 catalyzes the hydrolysis of C-terminal ubiquityl esters and amides that is critical for maintaining homeostasis in the neuronal cytoplasm. To explain, ubiquitin is a protein amply found in the body that aids in the regulation of other proteins and their functions. In further detail, UCHL1 activity is important as it removes ubiquitin from degraded proteins for recycling. The role of UCHL1 is particularly important not only due to the recycling of ubiquitin, but because the careful

regulation of the ubiquitin pathway is associated with many diseases and disorders. For instance, Liu et al. (2002) describes a form of Parkinson's diseases where the *Park5* gene induces a mutation in UCHL1 causing decreased ubiquitin hydrolase activity (Liu et al., 2002). Furthermore, UCHL1 is exclusively concentrated and expressed in neuroendocrine and neuronal perikarya and dendrites, and it is indiscernible in other cells (Lewis et al., 2010). As a result of the dense concentration of UCHL1 in nerve cells, distinct UCHL1 antibodies can be utilized as markers for neurons in immunohistochemical techniques. The upregulation of UCHL1, similarly to pNF-H, has been related to the degree of neurodegenerative disorders and damage affecting the CNS, more specifically, the expression of this protein is linked to the injury of motor neurons and the impairment of voluntary movements. As a result, the release profile of UCHL1 allows it to be readily detected from CSF and other fluids, such as blood; the concentration of UCHL1 in neurons is approximately three times greater than that of pNF-H, making the successful detection of this protein more probable after neurodegenerative damage. Thus, we later characterize UCHL1 as a potential indicator of neural tissue injury in the need to better evaluate neuroinflammation and nerve cell injury during and after an electrode implant.

2.5 Histology and Immunohistochemistry

2.5.1. Antigens and Antibodies

Immunohistochemistry has become a popular technique in neuroscience for the detection of cells in neural tissue. This technique is important for both monoclonal and polyclonal antibodies to determine antigens of interest in the detection of diseases or immune responses. In order to further understand the process of immunohistochemistry

and its relation to implanted Utah microelectrode arrays, we must first become familiar with its biological and chemical pathways.

As such, the principle of immunohistochemistry is to visually localize target cells in tissue sections through antigen tagging with specific antibodies. To explain, an antigen is a protein that is able to produce immune responses in the body; that is to say, antigens are harmful molecules that cause the immune system to produce antibodies (Abbas et al., 2012). Consequently, antibodies are substance that are induced by immune responses as a result of antigens. These are produced to recognize and aid in the removal of specific antigens from the body. The intimate relationships of antigen-antibody binding can be easily visualized through the use of a colored histochemical reaction that is apparent by light or fluorescent microscopy (Ramos-Vara & Miller 2014).

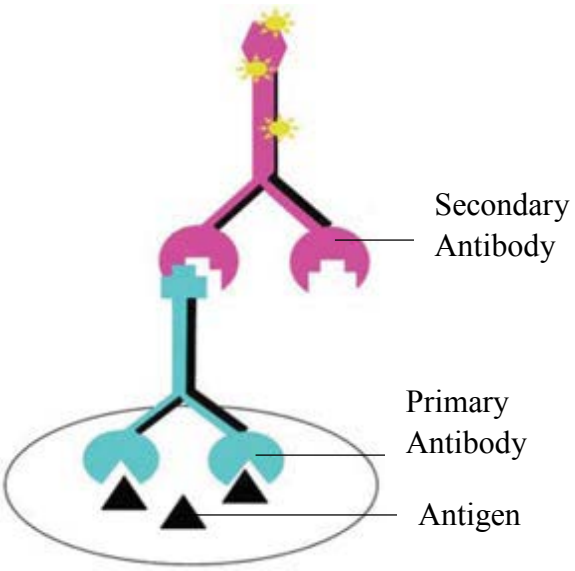

Figure 2.5: Immunohistochemical reaction between antibodies and antigens. (Hoffman et al., 2008).

Moreover, the avid and unambiguous relationship between antigens and antibodies allows it to be detectable through the use of immunohistochemistry. As illustrated in Figure 2.5, utilizing fluorophore-labeled secondary antibodies that tag the primary antibodies

bound to the antigens, enables the use of fluorescent microscopy as a means to visualize target cells. In other words, with this method of indirect fluorescent immunohistochemistry, the secondary antibody is labeled with a fluorescent molecule that can be seen using fluorescent light. The secondary antibodies used for fluorescent tagging must be compatible with its congruent primary antibodies, otherwise the stains will not function properly. As such, we explore different nuclear, neuronal, and non-neuronal proteins found in rat brains after injuries and successful perfusions.

2.5.2 Immunohistochemical Markers for Neuroinflammation

Different cellular markers and proteins were used to stain the cryosectioned brains to be able to distinctly visualize cellular expression in each section of tissue. Among these markers, the primary antibodies used to stain were NeuN, ferritin, ED1, and GFAP. To better understand how each of these markers function, we observed their expression in tissue sections were the injury caused by the microelectrode was visible. By studying histology in the tissue, we were able to observe the injury patterns and neuroinflammation that leads to cell recruitment and activation; more importantly, we can correlate the expression and activation of these cells to insertion injuries induced by the Utah arrays.

The neuronal nuclear protein, or NeuN, is usually found in nuclei and the perinuclear cytoplasm of nerve cells in the central nervous system (Gusel'nikova and Korzhevskiy 2015). Studies associated with NeuN have shown that this protein is solely found within nervous tissue, more specifically within the structure of a neuron; this protein primarily stains nuclei of mature nerve cell. (Gusel'nikova and Korzhevskiy 2015, Ünal-Çevik et al., 2004). As a result, this protein has been characterized as a positive marker for the analysis of neural injury, in this case it allows the analysis of nerve cell damage after

an electrode insertion. Moreover, as described on the methods section of this manuscript, NeuN was stained in combination with the glial fibrillary acidic protein (GFAP). This protein is a standard stain used to visualize reactive astrocytes. GFAP-positive cells are found around the entire tissue, but tend to aggregate further around the specific injury site. Astrocytes labeled with GFAP tend to have long projecting processes, which studies have described as activation and reactive gliosis (Szarowski et al., 2003). As such, GFAP was utilized in this study to observe reactive astrogliosis that occurs due to the destruction of nerve cells after injury in the central nervous system.

Furthermore, we focus on the levels of ferritin as an indicator of iron load in expressed microglia and macrophages. Ferritin has been described as a blood protein containing iron; this protein has been shown to increase and release free iron when there is damage to the blood-brain barrier or the central nervous system leading to hemorrhaging (Mehdiratta et al., 2008). This protein is often expressed in microglia and macrophages and it is released when there is need for iron sequestration after neural injury damages the BBB (Prasad et al., 2012). In addition, ferritin staining was done in correlation with ED1 stains. ED1 is a cellular marker that stains phagoctic microglia and active macrophages. Activated microglia cannot all be visualized with ED1 staining, as they are not all phagocytic; Iba1 is another cellular maker that can be used to stain all microglia in a brain section (Prasad et al., 2012). However, herein, we do not explore Iba1, but only focus on ED1 expression and activation of phagocytic microglia. As previously mentioned, microglia have been strongly correlated with neuroinflammation and cellular responses after neural injury (Fleming et al., 2006). Thus, visualizing activated glial cells will provide insight of how the injury affects the cellular response and inflammation cascade.

2.6 Significance

The importance of this study lies in understanding the effect and consequences of using microelectrodes as rehabilitative neuroprosthetic tools. Although this manuscript does not involve experiments around neural recordings with Utah arrays, assessing how neural tissue reacts to insertion injuries caused by these devices is equally as noteworthy. As a result, the significance of this study is to analyze axonal injury and cellular markers that are diagnostic of BBB, neural, and nerve cell damage, while assessing these responses in correlation to the insertion methods used to implant these devices.

Chapter 3: Materials and Methods

3.1 Experimental Design

All procedures were approved by the University of Miami Institutional Animal Care and Use Committee (IACUC). The experimental design of this manuscript revolves around assessing the acute effects of neural injury biomarkers, pNF-H and UCHL1, and immunohistochemical markers after rapid insertion of Utah microelectrode arrays. A temporal diagnosis of electrode-induced injuries provides insight into neural damage and neuroinflammatory patterns microelectrode array injury in both stab and implanted animal tissue.

Fifteen male Sprague-Dawley rats were subjected to a craniotomy in which five animals obtained the electrode implant for 4 weeks while the other ten animals received stab wounds for either 2 (5 animals) or 4 (5 animals) weeks. The stab wounds were induced with the same microelectrode arrays used in the implants. All animals received that exact same procedure and received blood draws by tail-vein puncture on the day of surgery and every 7 days until their time of euthanasia. The supernatant was separated and collected for use in ELISA. As a result, we hypothesize we will obtain the subsequent concentrations of pNF-H and UCHL1 at days 1, 7, and 14 for animals in the 2 week experiments and 1, 7, 14, 21, and 28 for animals in the 4 week experimental groups. The release profiles will be analyzed and compared between stab wounds and implants, as well as 2 and 4 week groups to obtain more detail about the up- and down-regulation of these markers. Lastly, the temporal assessment of pNF-H and UCHL1 will provide insight into their association with neuronal cell death and damage, as well as the injury severity and neuroinflammatory patterns caused by microelectrodes.

Moreover, histology analysis for a variety of cellular markers was performed on the extracted brain tissue from perfused animals. The tissue was embedded in gelatin and later cryosectioned to obtain both the control and experimental sides of the brain and draw comparisons of cell recruitment and activity at the injury site. Distinct cellular markers, such as GFAP, ferritin, NeuN, and ED1, will provide insight into the assessment of neuroinflammation and neural damage caused by microelectrodes. We suspect that animals with implanted arrays will have a stronger response to cell recruitment and activation as opposed to those who only received stab wounds. Due to previous successes in the diagnosis of neural injury from histology analyses, this data will also be compared to pNF-H and UCHL1 to weigh their capacity as viable cues for neural damage, including but not limited to electrode-induced injury. Further details on distinct experimental methods are highlighted below.

3.2 Microelectrode Implant Surgery

This procedure is similar to that described in Prasad et al., (2012). Sterile surgery was performed on all animals regardless of the procedure executed and all animals received the exact step-by-step routine craniotomy procedure that is explained below. The microelectrode arrays were also cleaned and sterilized per the manufacturer's recommendations for use in both implantation and stab injury. Prior to their use, the microelectrodes were washed with sterile distilled water and a 70% ethanol solution used as a disinfectant. Furthermore, before beginning surgery, each animal was anesthetized with 4% isoflurane and supplied with 2 L min^{-1} oxygen and kept deeply anesthetized throughout the entire length of the procedure (Prasad et al., 2012). After anesthesia was induced, a subcutaneous injection of Xylazine (5mg kg^{-1}, SQ) was administered to each

animal. Xylazine was given as a muscle relaxant and to maintain constant anesthetization throughout surgery (Prasad et al., 2012). After, the dorsal part of each animals' head was shaved with an automatic razor and swabs drenched in alcohol and iodine were used to clean the incision site. The animal was then carried and placed on a surgical pad that was used to cover the heating pad with which the animal was kept warm during the procedure. Before fixing the animal's head to the frame, an ophthalmic lube was applied to the eyes

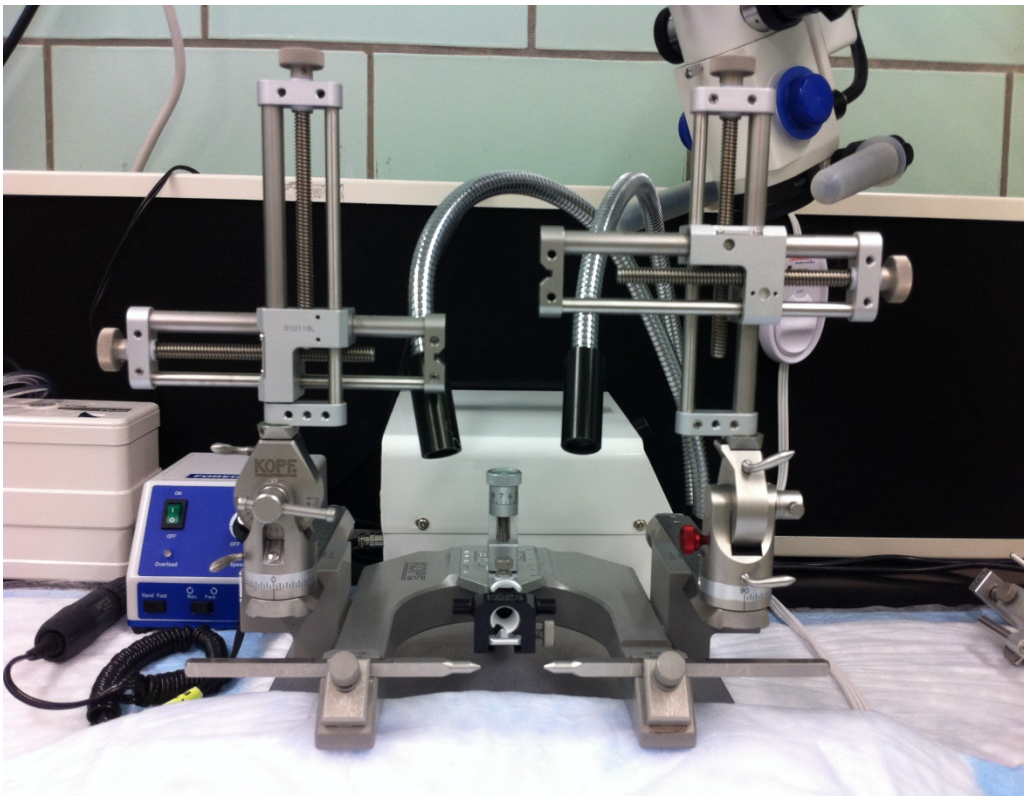

Figure 3.1: Small animal stereotaxic frame used for microelectrode implant surgery.

to keep them from dehydrating during the surgery. After, the head was fixed on a small animal stereotaxic frame as seen in figure 3.1 (Kopf Instruments, Tujunga, CA). Once the animal was completely stabilized on the frame, a mid-sagittal incision was made on the head between the eyes. Present connective tissue was removed using a surgical spatula until the skull became visible. Note that any and all excessive bleeding from the initial

incision was stopped with absorbent cotton balls and cleaned with hydrogen peroxide to assess the location of different landmarks on the skull. Moreover, a sterile marker pen was utilized to pin-point the exact positioning of support screws and the craniotomy site. It is important to highlight that animals with an electrode implant received 4 support screws, while animals with a stab injury only received 2 screws. The support screws are the attachment points for the dental acrylic that forms the head cap and covers the wound after surgery. Animals with an implant received more screws since it is more pivotal for the microelectrode to remain in place and not fall or move during the duration of the experiment until it is removed after perfusion. A fine drill bit (size 60) was used to make holes at the marked locations on the skull for the support screws (size 90), which were then inserted into the skull and stopped after 4 complete turns. After, a high-speed drill press (Kopf Instruments, Tujunga, CA) was used to carve out the site marked for the craniotomy (1mm lateral and 1.8mm posterior to bregma) on the somatosensory cortex (Prasad et al., 2012). The drill was not used continuously for more than 10 to 15 seconds. During wait periods, the skull was washed with sterile saline as to inhibit thermal injury during the drilling process. Once the bone at surgical site was unattached and thin enough, forceps were used to remove the small piece of skull and expose the cortex. In order to remove the dura mater, the outermost membrane encasing the brain and spinal cord, a 30-gauge needle was bent at an approximate 45° angle and used to puncture and carefully lift the dura. A microscissor was then used to cut and completely eradiate the dura at the electrode site allowing exposure of the cortical surface. Removal of the dura is a delicate procedure as imprecise cutting and lifting can result in further vascular damage and disruption of the BBB, so this portion of the surgery was executed under extreme precautions. After the

implant site was clear, the microelectrode array was manually positioned onto the cortex with small forceps. A microinjector was used to drop weight and push the electrode into the brain in one swift motion, aiding in an even and faster implant, which would later be

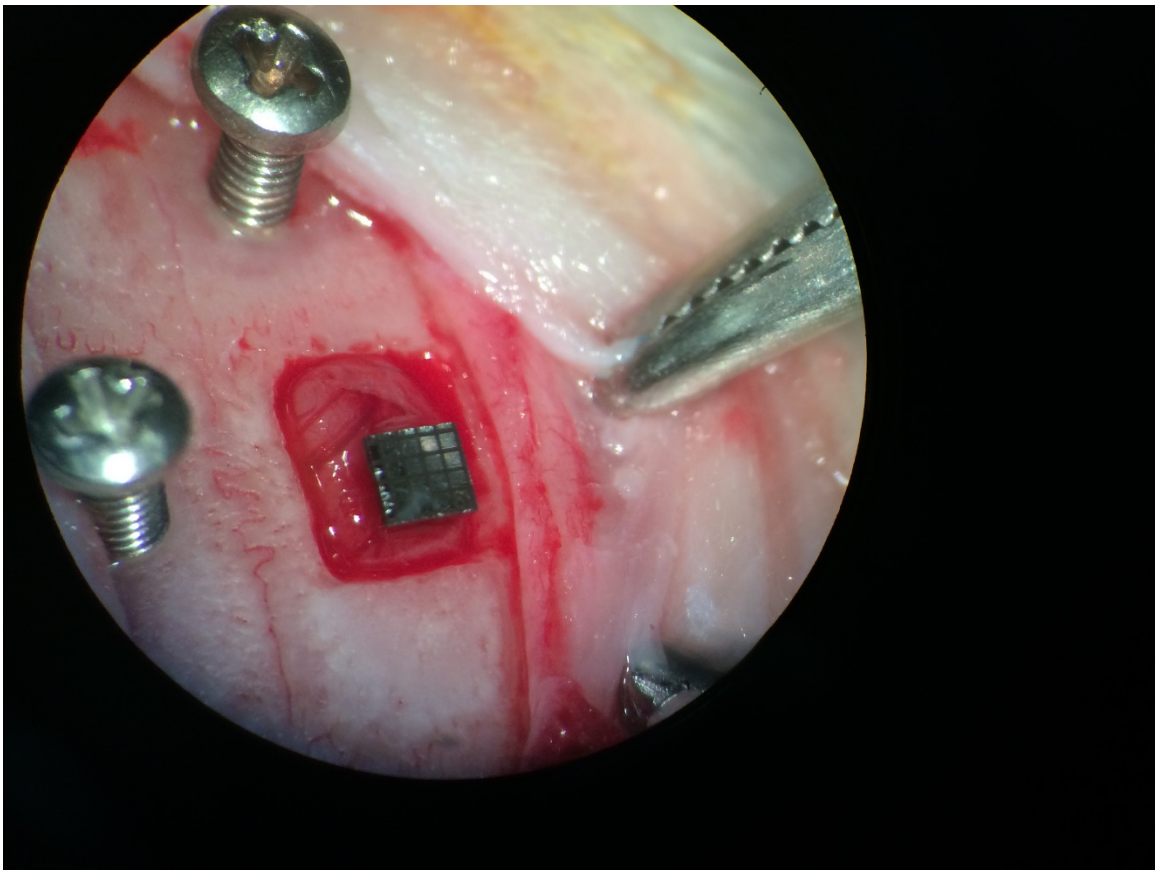

Figure 3.2: 16-Channel Utah microelectrode array positioned on the craniotomy site after removal of the dura matter.

assessed in terms on cellular responses. After, the electrode was either left in place if the animal was receiving an implant, or allowed to sit in the brain for approximately 5 minutes and then carefully removed from the tissue if the animal was receiving a stab injury. In both injury groups, however, all animals received the same treatment, aside from the duration the array was left in the brain. Furthermore, a small piece of gel foam was cut to the size of the craniotomy site and soaked with sterile saline. This was placed on top of the

injury and used as a separation layer between the injury and the dental acrylic cap. Dental acrylic (A-M Systems, Carlsborg, WA) was used to close the opening on the head as shown in figure 3.2. The head cap was carefully shaped and slowly crafted, such that the edges were smooth and the animals would not experience discomfort. After, Carprofen (5 mg kg^{-1}, SQ) was administered as an analgesic and anti-inflammatory at the end of surgery, and a repeated dose was given on the following day. Lastly, the animals were individually housed in newly sterilized cages that were placed on top of a heating pad for the animals to remain warm for up-to 2 hours post-surgery. The animals were constantly monitored for the entire duration of the day after the surgery was completed, and if necessary, hydrogen peroxide, sterile saline, or distilled water was used to maintain the head cap and surroundings clean from any remaining blood on that day and every week until perfusion.

3.3 Blood Collection

Blood was collected from each animal to evaluate the presence of chronic injury biomarkers, pNF-H and UCHL1, throughout the duration of the animal until euthanasia. The specifics for both pNF-H and UCHL1 are highlighted in chapter 2, section 2.5, subsections 2.5.1 and 2.5.2 of this manuscript, and for further detail on these proteins one should refer to those sections.

Blood collections were performed via tail-vein puncture for all animals 3 hours after surgery and every 7 days for a period of either 2 or 4 weeks, according to the duration of the experiment. In order to obtain blood, animals were placed into an anesthetizing chamber and anesthetized with 4% isoflurane and supplied with 2 L min^{-1} of oxygen. The animal's tail was massaged and warmed by hand before puncturing it with an 18-gauge needle. The needle was slowly inserted and removed until blood was freely flowing. The

tail was squeezed from one end to the other to facilitate the flow and collect blood into a 1.5 mL centrifuge tube, until there was approximately 1 mL of blood collected. Each sample was then centrifuged at maximum speed for 10 minutes to separate the supernatant from the precipitate. The clear supernatant was collected with a 100 μL pipet by parts, until no supernatant remained, and stored in another 1.5 mL centrifuge tube in a -20°C freezer. These samples were then used to run ELISA for protein expression levels of pNF-H and UCHL1.

3.4 Perfusion

All animals were euthanized via transcardial perfusion after either 2 or 4 weeks, according to their time points after surgery. Prior to perfusion, animals were deeply anesthetized with isoflurane (5%). Soon after, each animal received a subcutaneous injection of Ketamine/Xylazine, as to induce an overdose. An incision was made along the sternum and the chest cavity was lifted upwards and secured, so as to remain open. Consequently, the heart became exposed such that a needle was inserted through the left ventricle, while a hemostatic clamp was employed to fasten the heart with the needle still in place. A perfusion pump was then utilized to slowly push 1% PBS (phosphate-buffered saline) solution into the heart while a small incision was made in the right atrium of the animal's heart to excrete all fluids from the body. Utilizing the liver's red coloration change to a yellow hue as a cue for a successful perfusion, the pump was switched to deliver 4% paraformaldehyde (PFA) into the body. The PFA was used in tissue fixation to facilitate the removal of the brain tissue after perfusion. Once the perfusion was completed, the animal's head was separated from its body utilizing a guillotine. The brains were unveiled from the skull and kept in 4% PFA overnight, then transferred to 1×PBS overnight, and

later kept in 30% sucrose with sodium azide to cryoprotect the tissue, until ready for tissue embedding and cryosectioning.

3.5 ELISA

An ELISA, or an enzyme linked immunosorbent assay, was used for the detection of both pNF-H and UCHL1 in serum collected from all animals. The ELISA kits utilized were purchased from EnCor Biotechnology Inc Gainesville, FL. These kits are known as capture assays. They are designed in a 96-well format plate that is coated with an affinity purified mouse monoclonal antibody raised against either a purified recombinant human UCHL1 or against pNF-H, depending on the type of plate. According to the manufacturer's description of the plates, these are given a preservative and blocked with a protein solution that removes all other types of bindings to prevent the detection of other proteins present in the sample. Furthermore, the detections of proteins are obtained by incubating the standards and the experimental samples in the wells for 3 hours at room temperature. After this allotted time for incubation, another hour is allowed to pass for the protein to be captured by the antibody; note that this process can also be done overnight. Finally, the binding is detected by another antibody that is conjugated with horse radish peroxidase (HRP). Moreover, the reagent tetramethyl benzidine (TMB) is then added. This reagent produces a blue coloration in positive cells, a reaction which is stopped by adding sulfuric acid (H_2SO4) which turns the solution into a yellow color. Finally, the yellow signal that is produced after the reaction is stopped can be quantified with an ELISA plate reader, which gives absorbance measurements that are directly proportional to the concentrations of the detected proteins in the sample. Although the ELISA procedures were performed as explained above, the process requires further optimization and the results obtained from

the ELISA for our cohorts of animals are not used. In turn, the samples collected from the animals will be used as part of other experiments. However, in order to assess how axonal biomarkers are affected by microelectrode injuries, ELISA data from other cohort of animals was analyzed. These experiments involved the same surgical and implant procedures in 25 male Sprague-Dawley rats divided into acute, short-, and long-term time periods. The outcomes from the ELISA plates obtained from these animals are described in chapter 4.

3.6 Tissue Embedding

All rat brains, stab controls and implanted experimental animals, were embedded in 12% gelatin in 1×PBS with 0.1% sodium azide. The gelatin was warmed on a hot plate until dissolved, about 40°C for about 10 to 15 minutes. In the meantime, the brains were positioned dorsally and the frontal sections and cerebellums were cut in coronal sections and separated from the middle section of the brains as shown in figure 3.3. This allowed complete separation of the craniotomy site and the contralateral side to the injury from the rest of the brain tissue. The injury site and control side were embedded in a whole section and cut together to obtain a control side along with the experimental. After the gelatin was dissolved, plastic specimen containers were labeled with the rat ID and the orientation in which the tissue was embedded was marked. Gelatin was carefully pipetted into the bottom of the container, as to not obtain any air bubbles, and placed in the 4°C fridge until cooled and settled (approximately 10 minutes). During this time, the remaining gelatin was removed from the hot plate such that it would not be too warm to melt the gelatin at the bottom of the container on which the tissue would sit. Otherwise, if the gelatin is too warm, the tissue will sink to the bottom of the container and possibly crack during freezing due

to lack of insulation. Furthermore, after the gelatin base was cool, the tissue was oriented on top in the container, with the dorsal side facing upwards as seen in the orientation plane in figure 3.3. Soon after, enough gelatin was pipetted to cover the brain tissue and leave a portion of gelatin sitting on top of the brain. This process was carefully executed to not

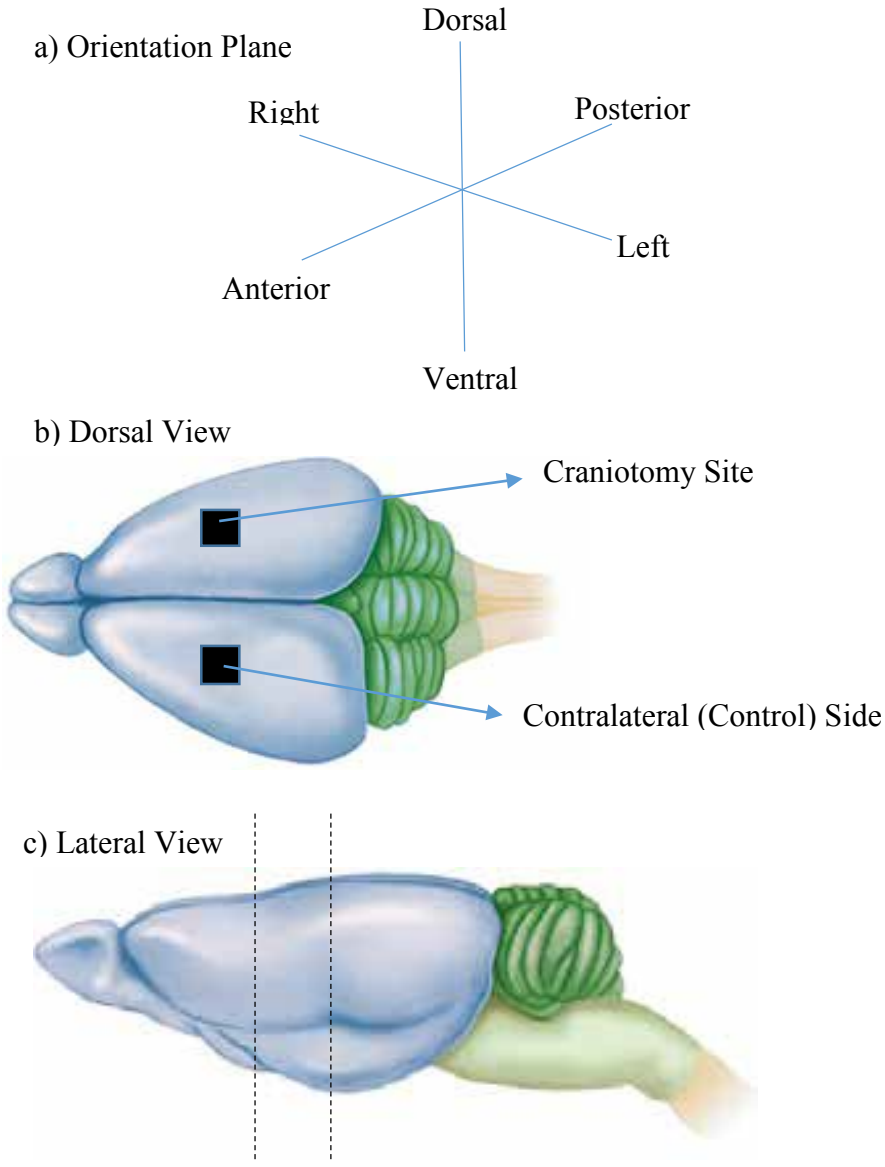

Figure 3.3: a) Two-Dimensional plane for orienting an animal brain. b) Dorsal view illustration of a common rat brain with the highlighted craniotomy and control sites. c) Lateral view illustration of a common rat brain highlighting a coronal cut passing through the brain, as was performed for tissue embedding. (Bear et al., 2004).

sink or obtain any air bubbles around the tissue which could affect freezing and cryosectioning later in the experiments. Once the tissue was completely embedded, the container was placed in the 4°C fridge for approximately 30 minutes of cooling, or until the gelatin was entirely solidified. The small container the tissue was embedded in was then placed in an airtight specimen cup overnight for freezing and cutting on the following day.

3.7 Freezing and Cryosectioning

Prior to freezing, all tissue was stored in a 4°C refrigerator in containers with 30% sucrose, acting as a cryoprotectant, and a small amount of sodium azide for a minimum of 24 to 48 hours.

A beaker was placed in a Styrofoam box that was filled with dry ice. After enough isopentane was poured into the beaker to be able to submerge an entire piece of embedded tissue. Small pieces of dry ice were added into the beaker, until the isopentane reached a temperature of approximately -57°C to -65°C, which was measured with a negative thermometer. The temperature was kept between -57°C to -65°C at all times during the freezing process, such that the tissue would not crack and was properly frozen. After, the gelatin block embedding the tissue was removed from the plastic container and the gelatin around the tissue was trimmed to obtain a smaller chunk. This process is vital to preserving the integrity of the tissue; if too much or too little gelatin is cut the brain may crack during freezing. Once the block was successfully trimmed, a chuck was stabilized inside the Styrofoam box with the dry ice and mounting media was poured onto the chuck. The tissue was then placed on top of the mounting media in the correct orientation and the mounting glue was allowed to solidify. After, the entire chuck was held with a pair of long forceps

and continuously dipped into the beaker with cold isopentane for freezing. Although the same process was followed in the embedding and freezing for all blocks, due to variability, the amount of times a chuck was dipped in isopentane differs according to the block's size. In other words, the larger or thicker a block, the longer it usually took to freeze. Thus, in order to assure that all tissues were completely frozen and did not crack, bubbles when the chuck was submerged in the isopentane were used as visual cues; in other words, if no bubbles emerged, the block was completely frozen, whereas if bubbles surfaced the tissue inside was not sufficiently cooled. All chucks were dipped into the isopentane for ten counts of 5 and ten counts of 10. After, if bubbles were still emerging from the tissue the tissue was dipped for consecutive counts of 5-7 until it was fully frozen.

Moreover, once the tissues were frozen and ready to cut, the cryostat was set at approximately -20°C and the chucks were placed inside to adapt to the chamber's temperature. During this time, slides were labeled from 1a thru 10a, 1b thru 10b, and 1c thru 5c for each tissue as shown in figure 3.4. The sections would be placed on the slides in series starting with slides "a", then "b", and lastly "c". By doing so, each slide would contain a spectrum of different depths within the tissue.

Furthermore, all chucks were sectioned in the same manner, they were placed and secured on the chamber before cutting. Once the first part of the block reached the blade, the excess gelatin covering the tissue was sectioned and disposed-of. No two blocks of tissue were sectioned using the same part of the blade nor glass, in order to avoid streaks and unevenness within the sections. This problem was also circumvented by cutting each section with one sweeping motion without stopping the blade in the middle of the section. No tissue was lost, since the sections were adhered to the slides as soon as the brain was

visible. This way, the injury was obtained from the very top of the brain for 100 consecutive sections, or 2 mm in depth. After cutting, the slides were placed on a slide warmer at 37°C for 5 minutes and then stored in labeled slide boxes inside a -20°C freezer until ready to stain.

Slides used in this direction →

Slide 1a	Slide 2a	Slide 3a	Slide 4a	Slide 5a	Slide 6a	Slide 7a	Slide 8a	Slide 9a	Slide 10a
0µm	20µm	40µm	60µm	80µm	100µm	120µm	140µm	160µm	180µm
200µm	220µm	240µm	260µm	280µm	300µm	320µm	340µm	360µm	380µm
400µm	420µm	440µm	460µm	480µm	500µm	520µm	540µm	560µm	580µm
600µm	620µm	640µm	660µm	680µm	700µm	720µm	740µm	760µm	780µm

Slide 1b	Slide 2b	Slide 3b	Slide 4b	Slide 5b	Slide 6b	Slide 7b	Slide 8b	Slide 9b	Slide 10b
800µm	820µm	840µm	860µm	880µm	900µm	920µm	940µm	960µm	980µm
1000µm	1020µm	1040µm	1060µm	1080µm	1100µm	1120µm	1140µm	1160µm	1180µm
1200µm	1220µm	1240µm	1260µm	1280µm	1300µm	1320µm	1340µm	1360µm	1380µm
1400µm	1420µm	1440µm	1460µm	1480µm	1500µm	1520µm	1540µm	1560µm	1580µm

Slide 1c	Slide 2c	Slide 3c	Slide 4c	Slide 5c
1600µm	1620µm	1640µm	1660µm	1680µm
1700µm	1720µm	1740µm	1760µm	1780µm
1800µm	1820µm	1840µm	1860µm	1880µm
1900µm	1920µm	1940µm	1960µm	1980µm

Figure 3.4: Placement of tissue sections onto slides by distance from the surface of the brain (µm). Slides are marked by series, beginning with series a, then b, and lastly c.

3.8 Immunostaining

Immunohistochemical staining was done over a two-day process, in which the primary antibodies were added on day 1 and the secondary antibodies on day 2; these are explained below. The slides chosen for staining were 1b, 5b, 1c, and 5c, accordingly. These slides were chosen since the "a" series, as shown in figure 3.4, contained fibrotic tissue that formed after the initial swelling from surgery and implantation diminished. This fibrotic tissue was seen all throughout the "a" series for all animals and no sign of the electrode injury was present. As a result, we chose slides from series' "b" and "c" and restarted the distance from the surface at slide 1b; in other words, slide 1b became 0 microns from the surface, such that the electrode injury fell within the range of slides 1b, 5b, 1c, and 5c.

3.8.1 Day 1: Primary Antibodies

During day 1 of the staining procedure, the slides were retrieved from the -20°C freezer and allowed to sit at room temperature for approximately 30 minutes to 1 hour. During this time, a fresh batch of 1×PBS was prepared by diluting a stock solution of 10×PBS with DI water. After, some PBS was poured onto a beaker and heated to 70°C on a plate warmer. Once the slides had been at room temperature for the time highlighted above, they were placed on a slide warmer at 37°C for 5 minutes. Meanwhile, moist paper towels were placed inside several slide boxes, on which the slides would sit for the remainder of the procedure. Moreover, after the 5 minutes had passed, the slides were placed atop the paper towels and a pap pen was used to create a hydrophobic layer around the tissue on each slide. Approximately 500µL of the warm PBS was then pipetted onto each slide and allowed to sit for 5 minutes, a process which was repeated twice. The warm PBS served to remove the gelatin from the sections and also aided in antigen retrieval. Two

different combinations of primary antibodies were made for the stained slides; 60 slides total were stained, half obtained rabbit ferritin and mouse ED1, while the other half received rabbit GFAP and mouse NeuN. Before applying the primary antibody solution, a blocking solution was made containing 0.5% Triton-X and 8% normal goat serum (NGS) of the total volume of solution made. The rest of the volume was filled with 1×PBS. Enough solution was made to pipet 0.5mL of blocking solution onto each slide. The blocking solution was left on the slide for a period of one hour on the closed slide boxes. After one hour, the slides were rinsed twice with 1×PBS for 5 minutes. After the rinsing, the primary antibody solution was prepared. The solution contained 0.5% Triton-X and 8% NGS, and either a ratio of 1:800 for GFAP and 1:500 for NeuN or 1:800 for ferritin and ED1, correspondingly. The rest of the total volume of the solution was fulfilled with 1×PBS. Lastly, 0.4mL of primary antibody solution was then pipetted onto each slide and incubated overnight in a 4°C fridge.

3.8.2 Day 2: Secondary Antibodies

On the second day of immunostaining, the boxes containing the slides were taken out of the 4°C fridge and placed at room temperature for a period of 30 minutes. After, the slides were rinsed with 1×PBS twice for 5 minutes and 3 times for 10 minutes consecutively. During this time, the secondary antibody solution was prepared. This solution contained 1:300 ratios of each secondary antibody, 1:1000 ratio of Hoechst, 1% NGS, and 1×PBS to dilute the mixture. The antibodies used were 488 goat anti-rabbit and 546 goat anti-mouse. Enough solution was prepared to pipet 0.4mL onto each slide. Before adding the secondary antibodies, a 1mL of solution containing only the Hoechst, NGS, and 1×PBS was pipetted into a 1.5mL centrifuge tube that already contained the antibodies.

This tube was centrifuged for 5 minutes to reduce the probability of fluorescent speckles on the sections. After that time, the supernatant was collected into another 1.5mL centrifuge tube and spun for an additional 5 minutes. The second supernatant containing the antibodies was then mixed with the rest of the stock solution to add onto the slides. The secondary antibody solution was then applied onto each slide and incubated for 1 hour at room temperature. After incubation, the slides were again rinsed with 1×PBS twice for 5 minutes and 3 times for 10 minutes consecutively. The slides were then placed on the slide warmer at 37°C for 5 minutes. Soon after, a small amount of Vectashield was applied on the four corners of each slide and a coverslip was placed on top of the sections. The slides were allowed to sit for approximately 10 minutes before a covergrip sealant was used to complete the slides. Lastly, all of the slides were stored in slide boxes inside the 4°C fridge until ready to be analyzed under the microscope.

3.9 Histopathology

All the stained slides were analyzed in the same manner, utilizing a Nikon Eclipse T*i* microscope with a Nikon intensilight C-HGFI and a digital sight camera model DS-U3. The software used to view and take pictures of the tissue sections was NIS-Elements version AR 4.40.00 64-bit. The slides were placed with the coverslip downward as this was an inverted microscope. After the light was turned on and, while on the bright field setting, the tissue was focused. The light was then turned off and the shutter was turned on to view the sections under fluorescent light. Photos were taken for each slide for all anima and included Dapi in blue, GFAP or ferritin in green, and NeuN or ED1 in red. These photos were saved and later analyzed on ImageJ, an image processing software developed by the

NIH. This software was used to count cells found on and around the injury or electrode holes, if visible within the tissue.

3.10 Analysis

Cell counting and area measurements were obtained through ImageJ. After, graphical data F-statistics were populated for each combination of animal groups through Excel 2016 as described in chapter 4 of this thesis.

Table 3.1: Step-by-step actions to measure fluorescent density or count particle

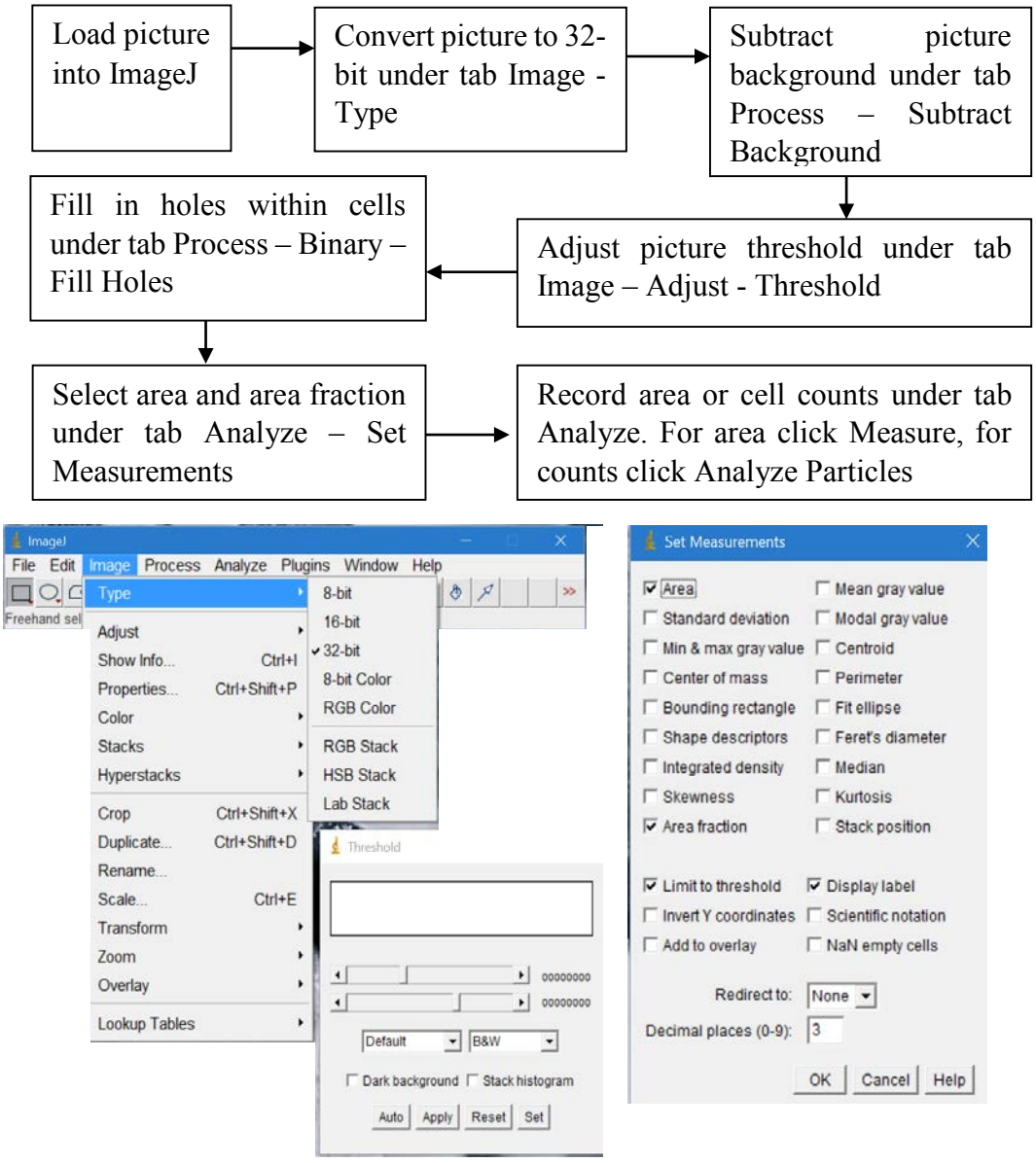

Figure 3.5: Cell and area counting actions on ImageJ.

Chapter 4: Results and Discussion

In this chapter we characterize the results obtained from the experimental design and methods of this thesis. As highlighted in section 3.6, ELISA and biomarker data obtained from other animal cohorts are presented. Since the electrodes used for those animal groups were functional, data from the array yield will also be looked at in correlation with biomarker expression. The histology assessment and immunostaining results from our experimental animals are evaluated.

4.1 Markers of Injury

4.1.1 Biochemical Analysis of Acute Implants

The purpose of analyzing injury biomarker data is to understand how a microelectrode and the length of an implant affects the neuroinflammatory response and nerve cell damage. In these experiments, readings for pNF-H and UCHL1 were obtained from blood and CSF in acutely implanted animals, as shown in figure 4.1.

Biomarker levels in acute animals are assessed separately from short- and long-term rats, since acute animals were euthanized almost immediately after surgery. The expression levels of pNF-H and UCHL1 showed very little variability among animals (figure 4.2). From this figure we also gathered that a fairly even relationship was observed for each marker amongst all the acute rats and we attribute the minimal differences in concentration to the different biotic and abiotic factors affecting the animals and implant sites (Prasad et al., 2011, Prasad et al., 2012, Prasad et al., 2014). More importantly, figure 4.1 showed no significant difference of both pNF- H and UCHL1 in CSF and blood. Blood withdrawals are overall easier and less invasive than CSF, making the resemblance of injury biomarkers between the two fluids highly significant for assessing CNS damage.

Furthermore, although CSF samples were also acquired for short- and long-term animals, these are not discussed here, since from our acute animals and previous studies we can conclude that expression levels of pNF-H and UCHL1 in serum and CSF are comparable (Lewis et al., 2010, Prasad et al., 2012, Shaw et al., 2005, Siman et al., 2008). As such, for short- and long-term rats we analyzed the variability of pNF-H and UCHL1 in blood among all animals in comparison to the electrode array yield as a means to assess electrode performance.

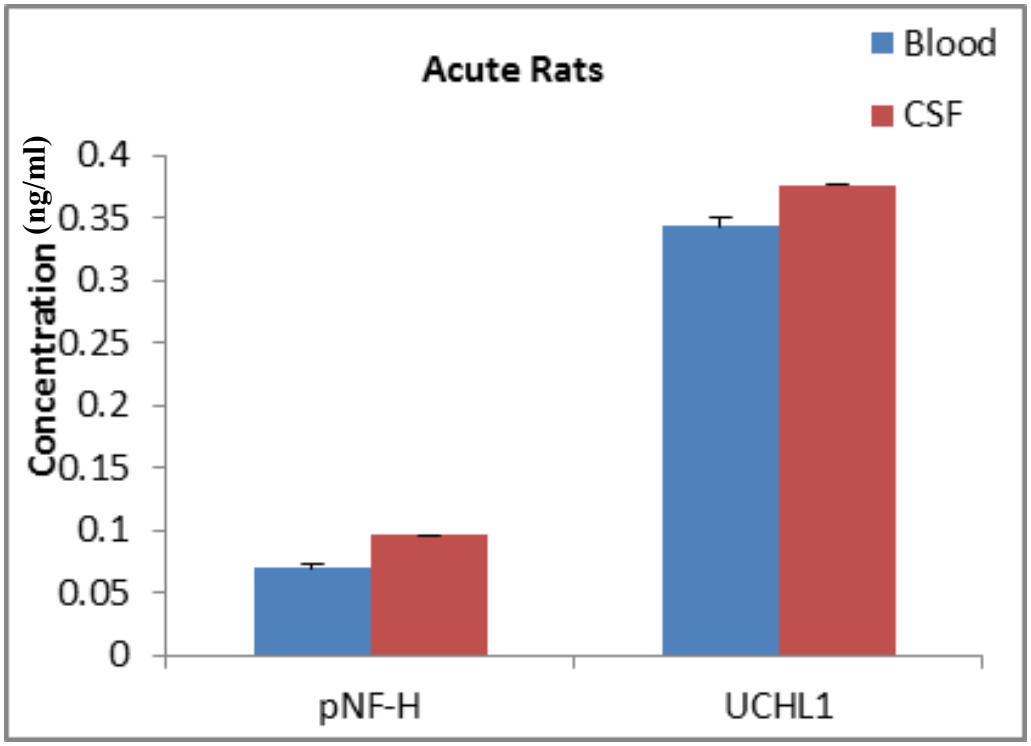

Figure 4.1: Comparison of average pNF-H and UCHL1 in blood and CSF of acutely implanted animals. Standard deviation is of the average values of each biomarker for all acute animals.

(a)

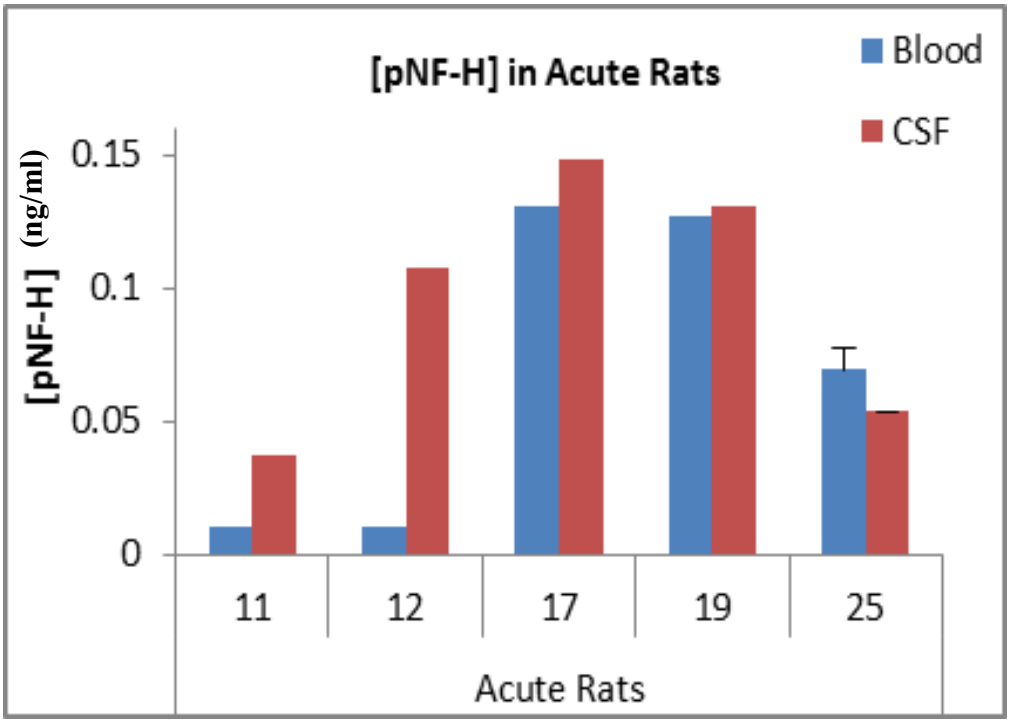

(b)

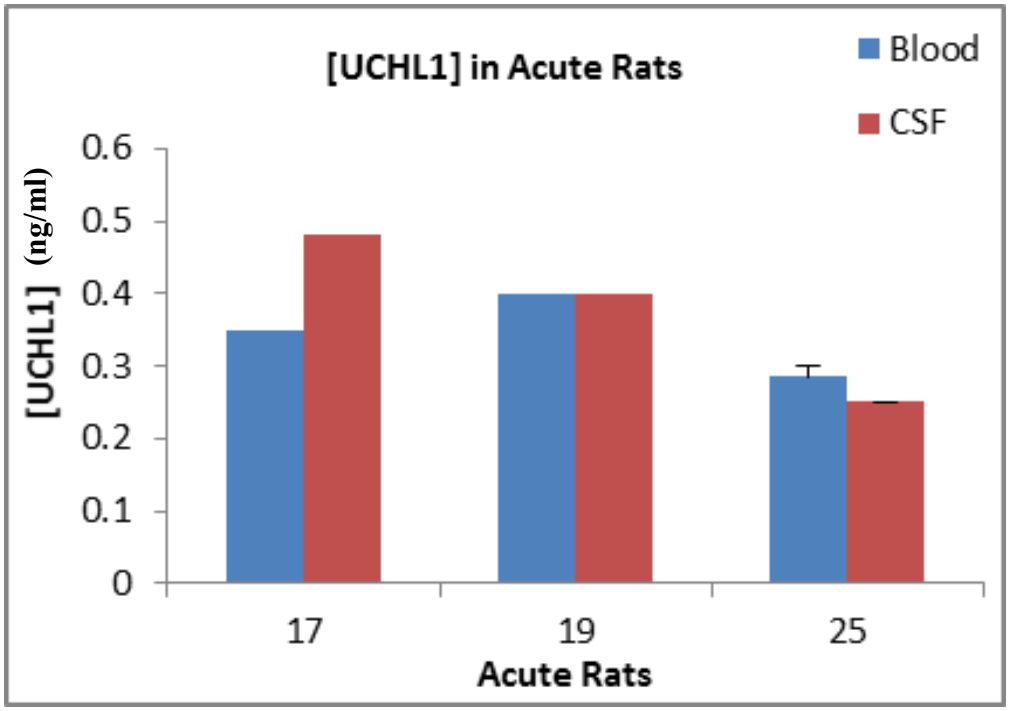

Figure 4.2: (a) Comparison of pNF-H detection in blood and CSF for acute animals. (b) Comparison of UCHL1 detection in blood and CSF acute animals.

4.1.2 Temporal Evolution

From this experimental setting, 3 longest-term animals were chosen. The temporal evolution for pNF-H and UCHL1 is individually assessed for rats 4, 9, and 13, as shown in figure 4.3 below. The temporal assessment allowed us to understand the fluctuations in concentration for each of these markers. Animals 4, 9, and 13 show continuous presence of pNF-H and UCHL1, suggesting the ongoing axonal, nerve cell damage and cellular

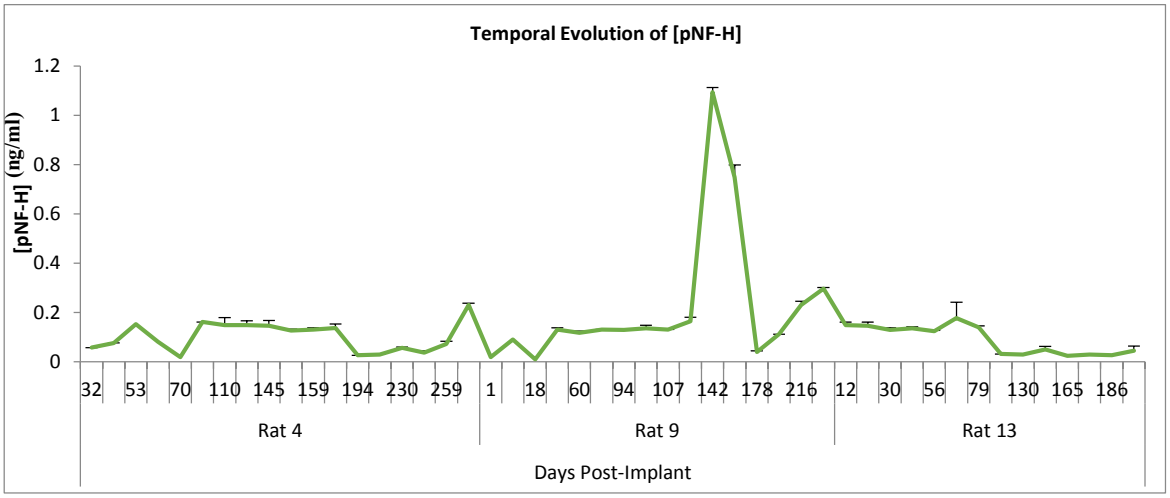

(a)

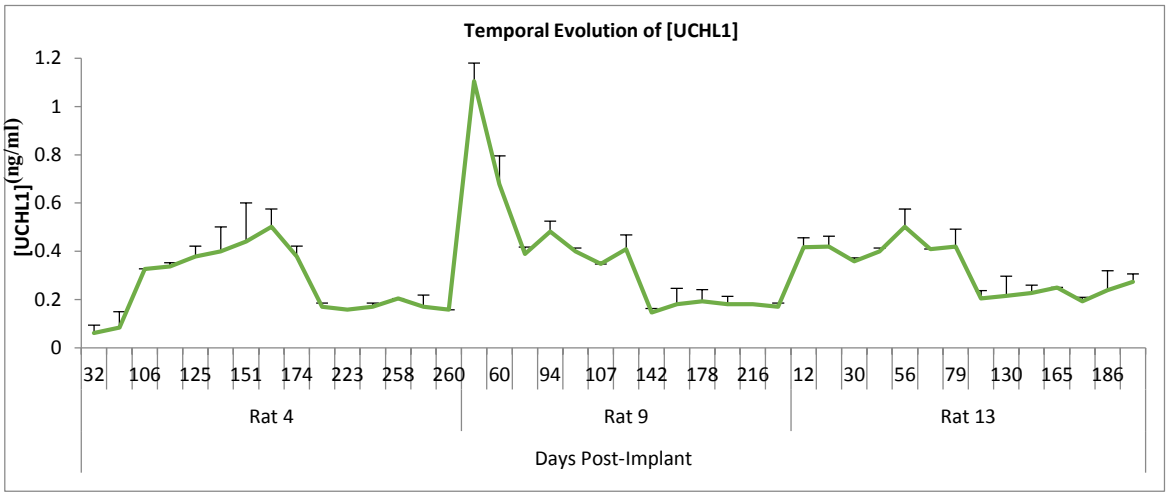

(b)

Figure 4.3: (a) Temporal evolution of pNF-H in long-term animals R4, R9, and R13. (b) Temporal evolution of UCHL1 in long-term animal R4, R9, and R13.

injury that extends into the chronic period, due to the presence of the electrode in the tissue. Animal 9, which shows an increase in both of these markers at different time points can indicate a disturbance in the tissue that caused a spike in expression of these proteins.

Herein, we show that after an electrode implant, whether or not there is failure, surrounding tissue may become inflamed and other neural factors injured during the surgical or implant time (Prasad et al., 2011, Prasad et al., 2012, Prasad et al., 2014). As a result, we experienced increased levels of chronic injury biomarkers in animals with substantial post-implant intervals (figure 4.3). In addition, from the temporal evaluation of the post-implant times in R4, 9, and 13 we visualize an overall decrease in both markers, most likely attributed to a stabilized injury response. However, the values of either biomarker was significant enough to suggest further axonal degeneration even after the expression levels diminished (Dash et al., 2010, Papa et al., 2010, Prasad et al., 2012, Siman et al., 2008). As such, this biomarker data is too problematic to make a final conclusion on whether these are good indicators of microelectrode-induced neural injury, despite their release after neuronal damage.

4.1.3 Coupling Functional and Biochemical Factors

The association between injury marker expression and electrode yield is illustrated in figure 4.3, where array yield is the fraction of electrodes within an array that isolated single action potentials. This assessment displays the overall relationship between a high percent array yield signifying good electrode performance and the manifestation levels of both pNF-H and UCHL1. From this comparison, we expect an indirectly proportional relationship between these two factors, thus remaining consistent with the characteristics surrounding electrode failure. Figure 4.3 (a) and (b) both show that animals with good array

yields, whose electrodes did not experience failure, had lower or poor biomarker expression. In the meantime, animals with lower yields presented higher concentrations of pNF-H and UCHL1, indicative of a stronger injury and tissue response.

The functional aspects of the implanted arrays are important to understand the implants effects on the tissue. Thus, the cross comparison of electrode array yield and chronic injury biomarkers gave notice to how electrode performance affects the neuroinflammatory response and, in turn, the biochemical data that responds to neural

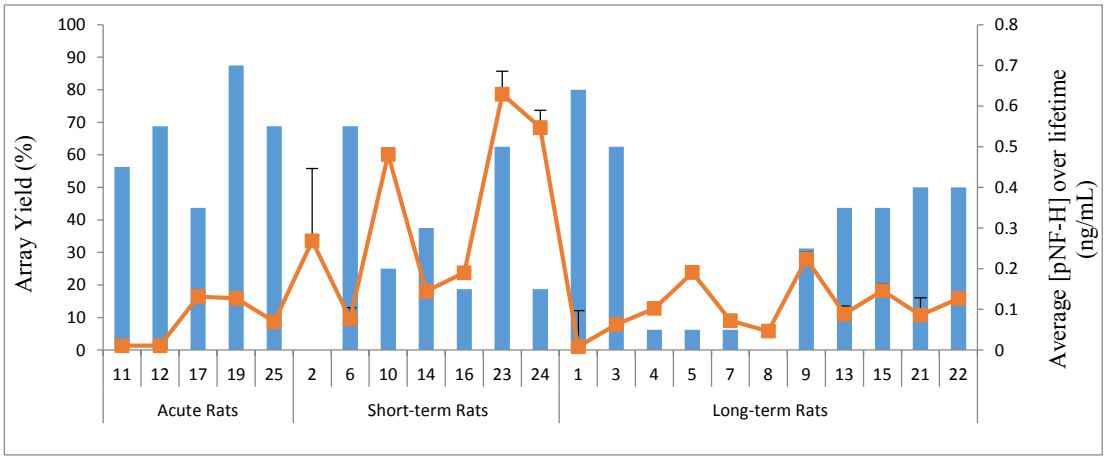

(a)

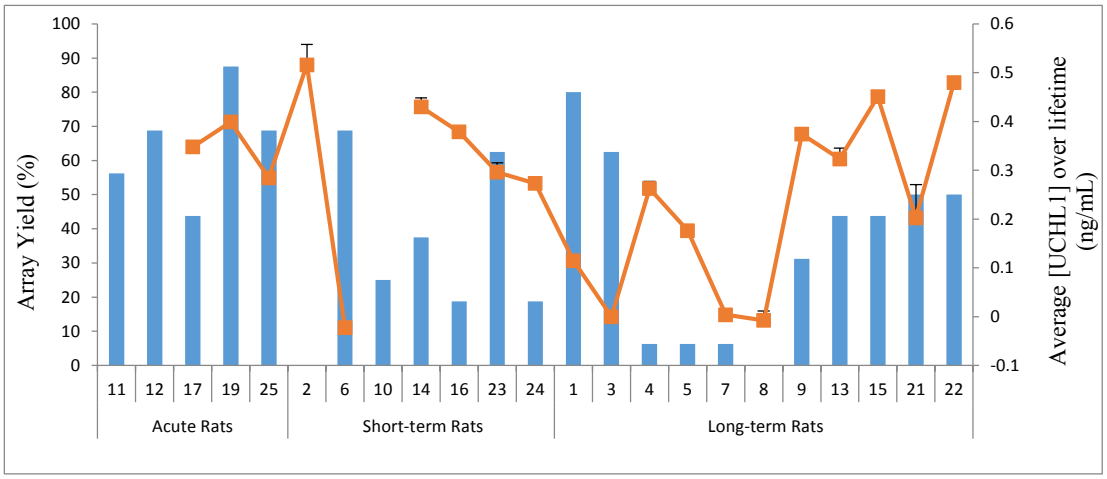

(b)

Figure 4.4: (a) Percent array yield and pNF-H concentration in acute, short-term, and long-term animals. (b) Percent array yield and UCHL1 concentration in acute, short-term, and long-term animals.

damage (Prasad et al., 2012). A relatively good electrode array tends to have poor upregulation of injury markers, while a poor electrode array has high expression of injury markers. These results, illustrated in figure 4.4, correspond to how the varying functionality of the implant affects surrounding tissue and generates an injury response from reduced neuronal integrity (Prasad et al., 2011, Prasad et al., 2012, Prasad et al., 2014). Based on these results, we can conjecture that pNF-H and UCHL1 can progressively be utilized to recognize different levels of neuroinflammation and neural injury in combination with determining electrode performance.

4.2 Immunohistochemistry

Observing data for the different immunohistochemical markers in electrode-injured animals leads to several assumptions about tissue response of and around the injury. Herein, our major results focus on the expression of the following markers of neuroinflammation: ferritin, ED1, GFAP, and NeuN.

As an indirect marker of free iron detected in microglia and macrophages, ferritin expression is characteristic of hemorrhaging and blood-brain barrier damage (Mehdiratta et al., 2008, Prasad et al., 2012). As seen in figure 4.5, ferritin levels in four-week stab animals appear overall higher than in two-week animals; however, there was no statistical difference between these groups (p-value = 0.11 > 0.05), a factor which can be attributed to the initial damage created from insertion of the microelectrode. The small differences in ferritin levels may be caused by the extended time-span of one animal cohort versus the other that led to microhemorrhaging. The evaluation of free iron present in microglia and macrophages can be directly correlated to ED1 expression in stab animals. From figure 4.6, we gather that there is significant difference in ED1 between four and two-week stab

animals (p-value = 0.001 < 0.05). Herein, four-week stabs show a higher fluorescent density of ED1 than two-week stabs, a factor that can be credited to the ongoing neuroinflammatory response (Biran et al., 2005). Although our data suggests more activated microglia and macrophages in four-week stabs through ED1, there was no significant difference in ferritin levels for these groups. To explain, higher ED1 expression in four-week than in two-week animals suggests there is an ongoing foreign body response leading to activated microglia and macrophages on the tissue. This, however, is not seen for ferritin; instead, four- and two-week animals express similar levels of free iron. Unlike activated microglia, which are one of first responders to injury, ferritin expression suggests that vascular disruption and BBB damage only appears to be present during the initial insult with the electrode. It is at the time of insertion and hours post-insertion that we expect an increase in free iron that is visible through ferritin staining. This may be partially due to activated microglia that are constantly recruited as a result of reactive gliosis that can persist for several weeks or months post-injury (Biran et al., 2005, Fernández et al., 2014, Fleming et al., 2006, Polikov et al., 2005, Szarowski et al., 2003). Prolonged microglia and macrophage activation is also consistent with the characteristic release of pro-inflammatory factors that aid in the chronic inflammatory response, a variable that can lead to more fibrotic tissue growth at the surface of the electrode.

Moreover, in comparing the two stab wound cohorts, we can also refer to figure 4.7 which exemplifies the density of GFAP. Statistical data for this protein suggests no significant difference between the groups (p-value = 0.46 > 0.05); this indicates that there is a fairly equal astrocyte reactivity at the site of injury. Comparable astrocyte expression between two- and four-week animals may be attributed to the acute time points of our

cohorts. In other words, our timespans do not capture astrocytic encapsulation since it is not completed until six to eight weeks post-implantation (Polikov et al., 2005). Reactive astrocytes are known to encapsulate and engulf the electrode or site of injury; in other words, GFAP-positive cells can be found all around the tissue, however reactive astrocytes, characteristic of long, projecting processes that intermingle with other cells, further aggregate and create a sheath that encapsulates the injury site (Biran et al., 2005, Szarowski et al., 2003, Turner et al., 1999). Astrogliosis has been previously associated with the neuroinflammatory response and said to increase during the destruction of nerve cells after CNS injury. The accumulation of activated microglia and reactive astrocytes can also result in a process known as "frustrated phagocytosis", which is characterized by increased inflammation and possible neuron death (Biran et al., 2005). Finally, in stab animals we see a statistically significant difference of NeuN in figure 4.8, where longer-term animals had a higher count of neuronal nuclei (p-value = $0.001 < 0.05$). During the beginning of the foreign body response, after the initial insult with the electrode, there is evidence of a "blackout period" in which no signals should be able to be recorded if using a functional array (Prasad et al., 2011). This "blackout period" is characterized by low neuronal yield, such that there are is not much electrical activity that can be acquired within the first two weeks, after which we see an increase in neurons (Prasad et al., 2011).

Furthermore, a statistical comparison of four-week animals (stab and implant) showed no significant difference since all their calculated p-values were > 0.05 (figures 4.13-4.16). This is consistent, when analyzing figures 4.9-4.12 comparing two-week stab with four-week implant animals, which showed the same results from comparing the two cohorts of stab wounds (figures 4.5-4.8). Thus, from our results we see that ferritin, as well

as GFAP show no significant difference between four- and two-week groups, while ED1 and NeuN are higher for four-week than two-week animals.

At the electrode surface, these arrays consist of a bulky substrate that may increase pressure, vessel rupturing, and neuroinflammation leading to higher levels of glial reactivity at the top of the injury. Typically, this substrate can cause an increased cellular response as part of additional forces and foreign material that prolong injury at the surface of the brain. As such, it is closer to the electrode surface (0-100μm) that we expect to see greater levels of glial activity and free iron. For instance, although our results show no significant difference in astrocyte proliferation for all animal groups, there are signs of increased reactivity from 0 to 600 microns when compared to sections closer to the recording tip (800-1480μm). Based on our data, the main contributing factor to our immunohistochemical results appears to be the insertion speed with which our arrays are implanted. One of the main differences between this experiment and other microelectrode studies is that our arrays are rapidly inserted with the help of a microinjector. Much like Biran et al, (2005), other electrode studies have not considered the penetrating injury from electrode implants a significant long-term contributing factor of the neuroinflammatory response. However, their insertion speed for implanting electrodes was slow, which they have noted not to play a major role in brain tissue responses. Based on our results, however, we have observed that the initial insult caused by rapid insertion of Utah arrays may be an important contributing factor of neuroinflammation. This is corroborated by data from our four-week stab and implant animals, which indicate that neuroinflammation is present one month after surgery and that the foreign body response, cellular encapsulation, and fibrosis are part of the initial injury caused by insertion of the array.

4.2.1 Two- and Four-Week Stab Animals

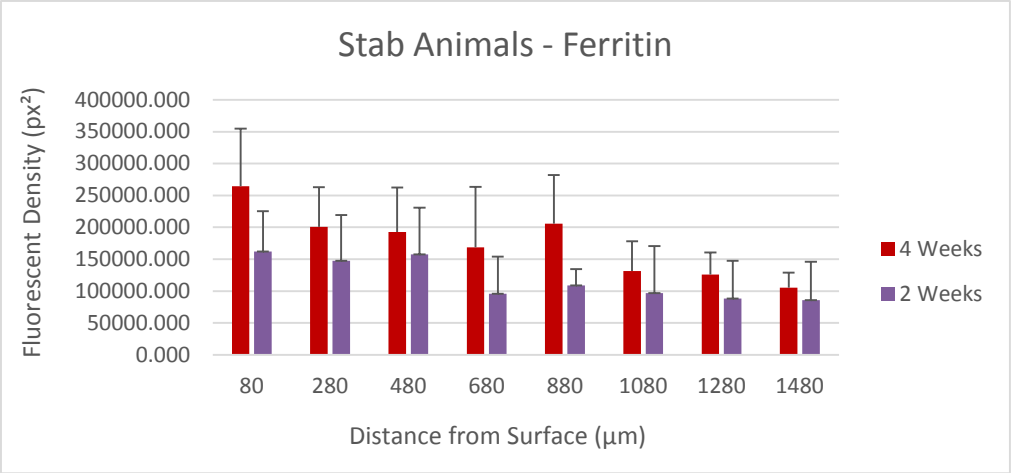

Figure 4.5: Average ferritin fluorescent density per brain section for five two-week and four four-week stab animals. Although higher levels of free iron in present microglia and macrophages are visible for four-week animals, there was no significant difference (p-value = 0.11 > 0.05, $F < F_{critical}$). The fluorescent density for each tissue section used is out of 4,915,200 px^2. Standard deviation is of the average fluorescent density per tissue section.

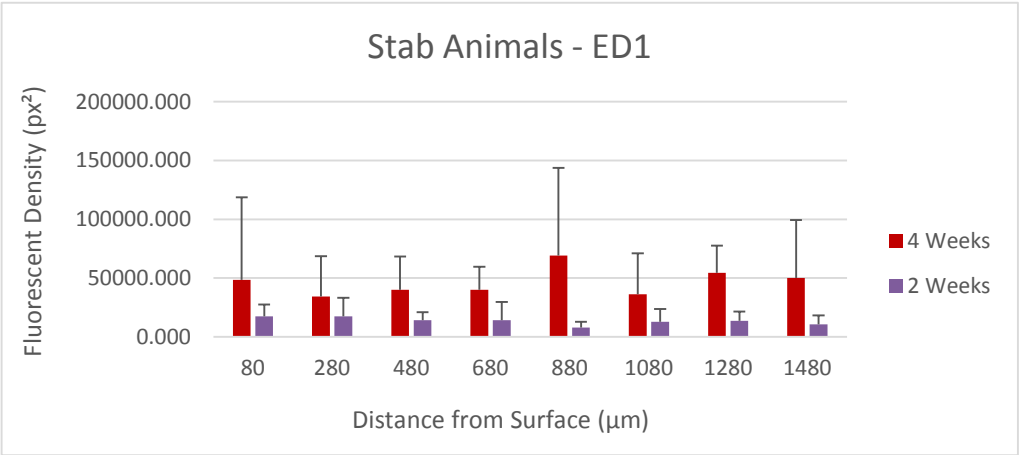

Figure 4.6: Average ED1 fluorescent density per brain section for five two-week and four four-week stab animals. Higher density of activated phagocytic microglia and macrophages are seen for four-week animals; this difference is statistically significant (p-value = 0.001 < 0.05, $F > F_{critical}$). The fluorescent density for each tissue section used is out of 4,915,200 px^2. Standard deviation is of the average fluorescent density per tissue section.

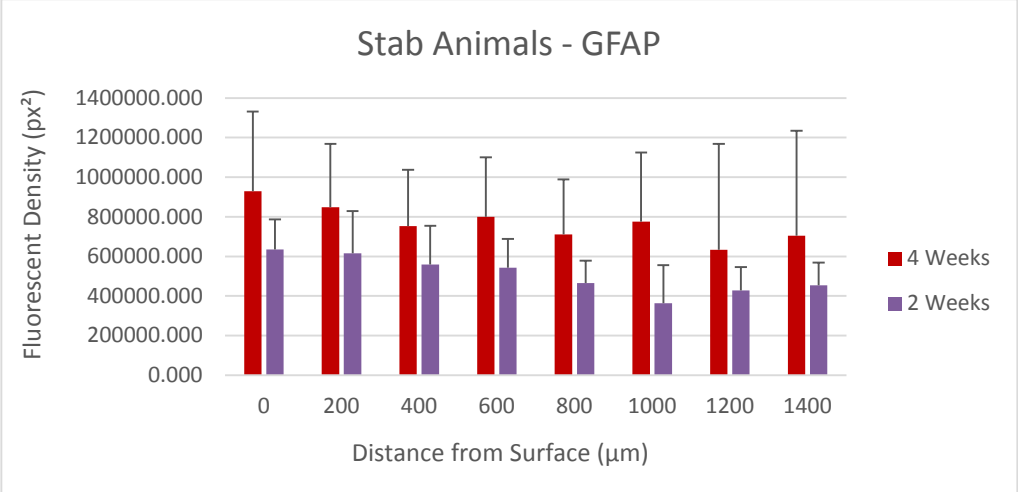

Figure 4.7: Average GFAP fluorescent density per brain section for five two-week and four four-week stab animals. Although higher levels of reactive astrocytes or $GFAP^+$ cells are visible for four-week animals, there was no significant difference (p-value = 0.46 > 0.05, $F < F_{critical}$). The fluorescent density for each tissue section used is out of 4,915,200 px^2. Standard deviation is of the average fluorescent density per tissue section.

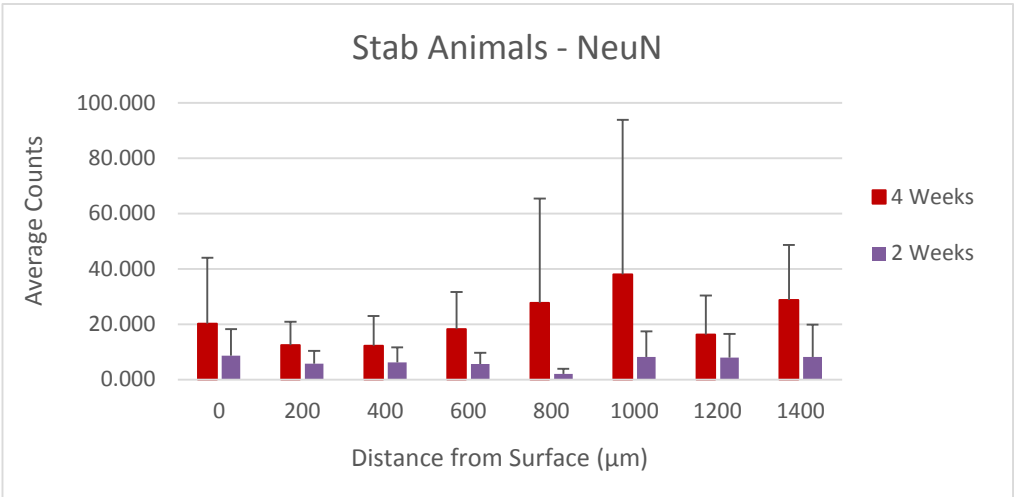

Figure 4.8: Average NeuN counts per brain section for five two-week and four four-week stab animals. Higher counts of neuronal nuclei are seen for four-week animals; this difference is statistically significant (p-value = 0.001 < 0.05, $F > F_{critical}$). Standard deviation is of the average counts per tissue section.

4.2.2 Two-Week Stab and Four-Week Implant Animals

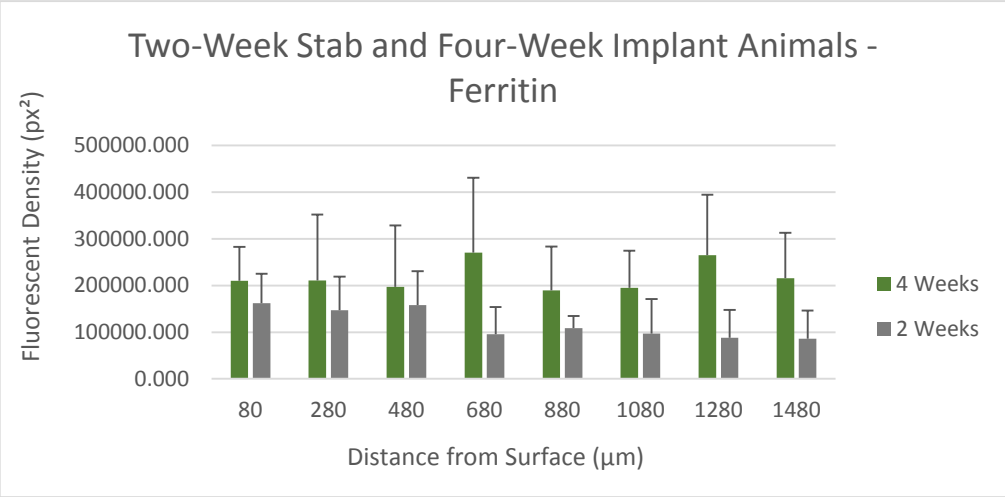

Figure 4.9: Average ferritin fluorescent density per brain section for five two-week stab and five four-week implant animals. Although higher levels of free iron in present microglia and macrophages are visible for four-week animals, there was no significant difference (p-value = 0.46 > 0.05, $F < F_{critical}$). The fluorescent density for each tissue section used is out of 4,915,200 px^2. Standard deviation is of the average fluorescent density per tissue section.

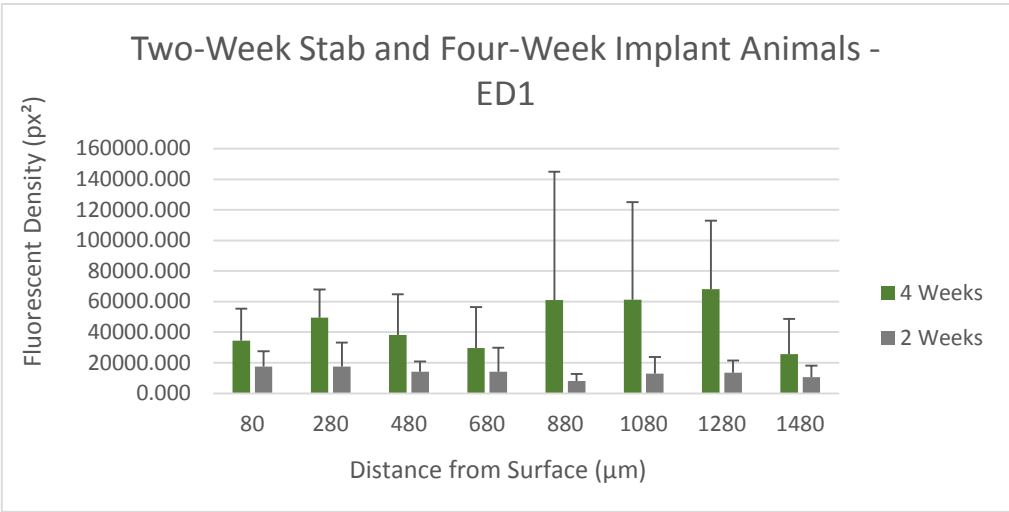

Figure 4.10: Average ED1 fluorescent density per brain section for five two-week stab and five four-week implant animals. Higher density of activated phagocytic microglia and macrophages are seen for four-week animals; this difference is statistically significant (p-value = 0.0001 < 0.05, $F > F_{critical}$). The fluorescent density for each tissue section used is out of 4,915,200 px^2. Standard deviation is of the average fluorescent density per tissue section.

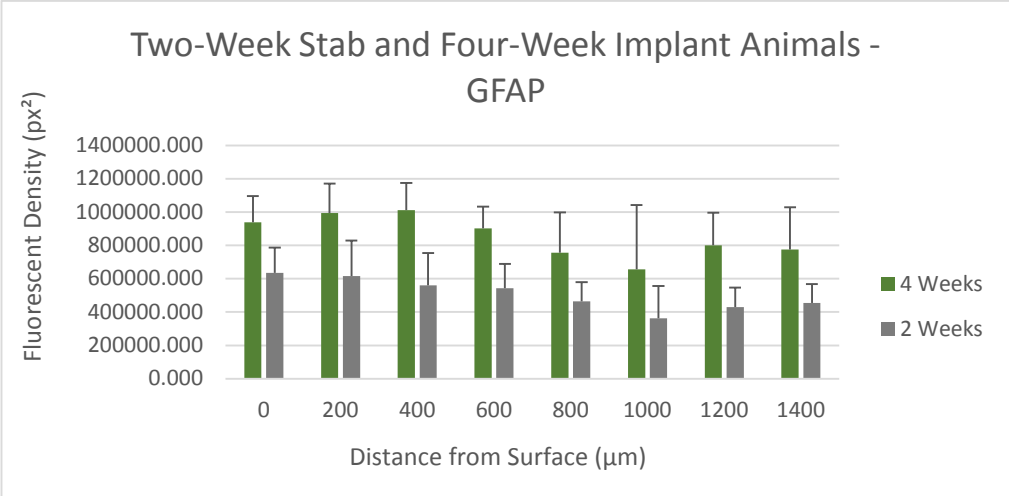

Figure 4.11: Average GFAP fluorescent density per brain section for five two-week stab and five four-week implant animals. Although higher levels of reactive astrocytes or $GFAP^+$ cells are visible for four-week animals, there was no significant difference (p-value = 0.23 > 0.05, $F < F_{critical}$). The fluorescent density for each tissue section used is out of 4,915,200 px^2. Standard deviation is of the average fluorescent density per tissue section.

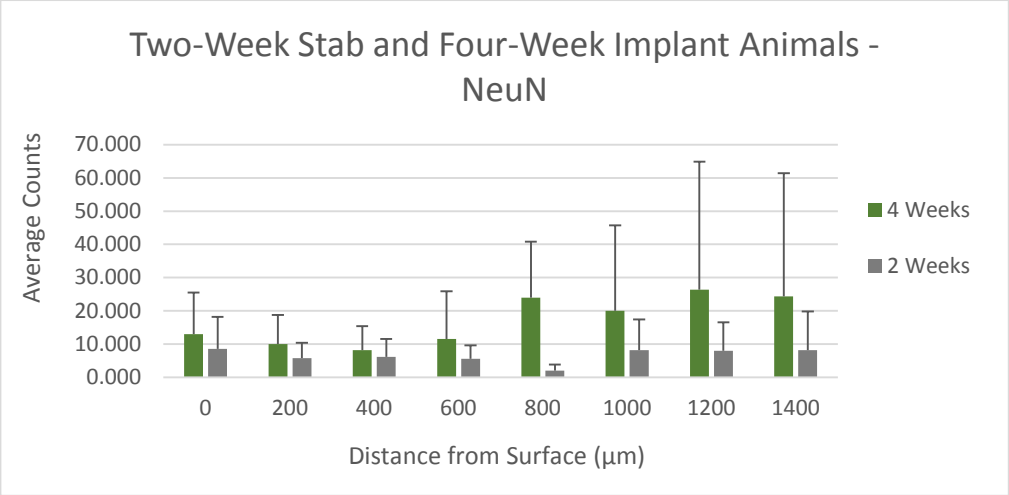

Figure 4.12: Average NeuN counts per brain section for five two-week stab and five four-week implant animals. Higher counts of neuronal nuclei are seen for four-week animals; this difference is statistically significant (p-value = 0.002 < 0.05, $F > F_{critical}$). Standard deviation is of the average counts per tissue section.

4.2.3 Four-Week Stab and Implant Animals

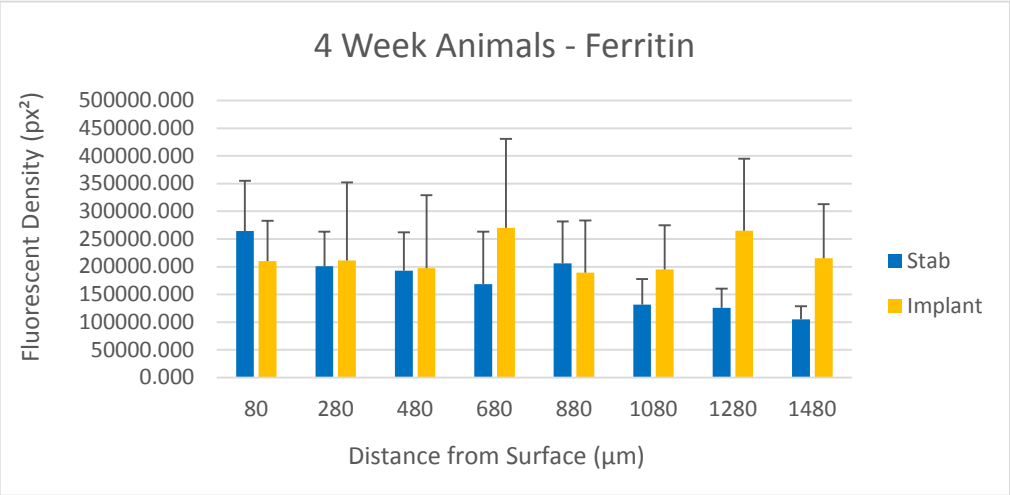

Figure 4.13: Average ferritin fluorescent density per brain section for four four-week stab and five four-week implant animals. No significant difference is seen in the levels of free iron in present microglia and macrophages between four-week stab and implant animals (p-value = 0.09 > 0.05, $F < F_{critical}$). The fluorescent density for each tissue section used is out of 4,915,200 px^2. Standard deviation is of the average fluorescent density per tissue section.

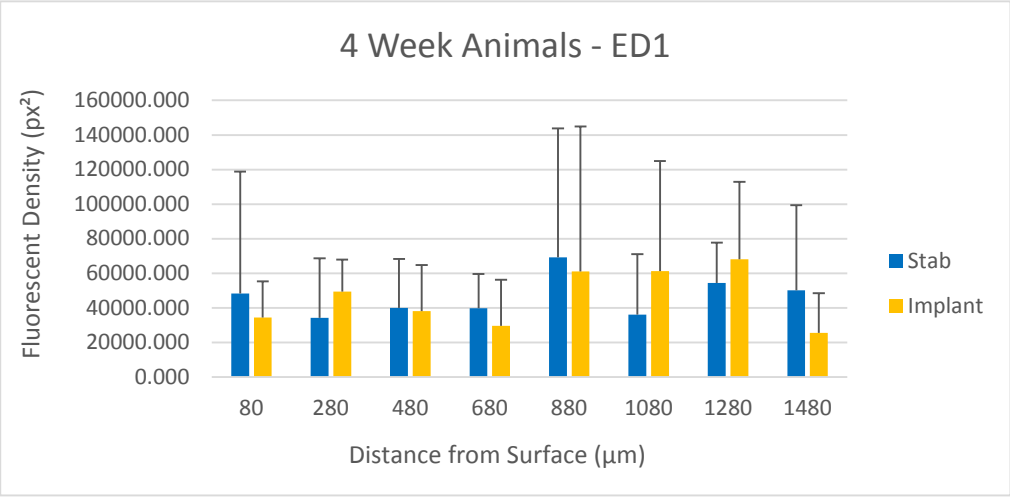

Figure 4.14: Average ED1 fluorescent density per brain section for four four-week stab and five four-week implant animals. No significant difference is seen in the density of activated phagocytic microglia and macrophages between four-week stab and implant animals (p-value = 0.19 > 0.05, $F < F_{critical}$). The fluorescent density for each tissue section used is out of 4,915,200 px^2. Standard deviation is of the average fluorescent density per tissue section.

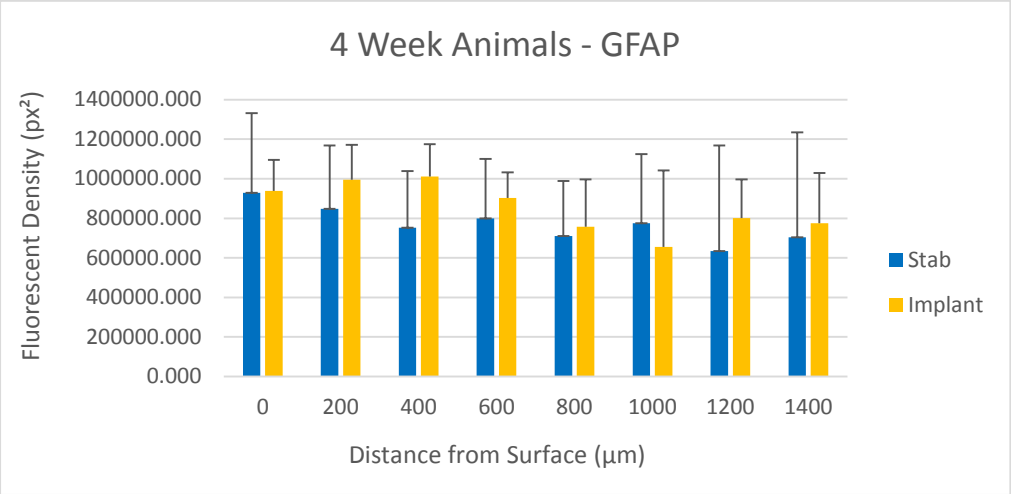

Figure 4.15: Average GFAP fluorescent density per brain section for four four-week stab and five four-week implant animals. No significant difference is seen in the density of reactive astrocytes or $GFAP^+$ cells between four-week stab and implant animals (p-value = 0.21 > 0.05, $F < F_{critical}$). The fluorescent density for each tissue section used is out of 4,915,200 px^2. Standard deviation is of the average fluorescent density per tissue section.

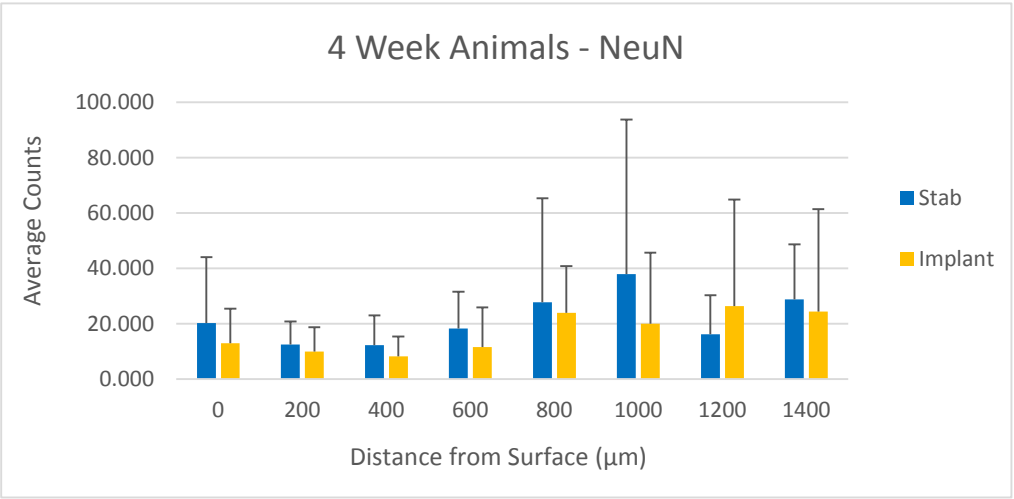

Figure 4.16: Average NeuN counts per tissue section for four four-week stab and five four-week implant animals. No significant difference is seen in the counts of neuronal nuclei between four-week stab and implant animals (p-value = 0.29 > 0.05, $F < F_{critical}$). Standard deviation is of the average counts per tissue section.

4.3 Supplementary Data

4.3.1 Two-Week Stab Animals

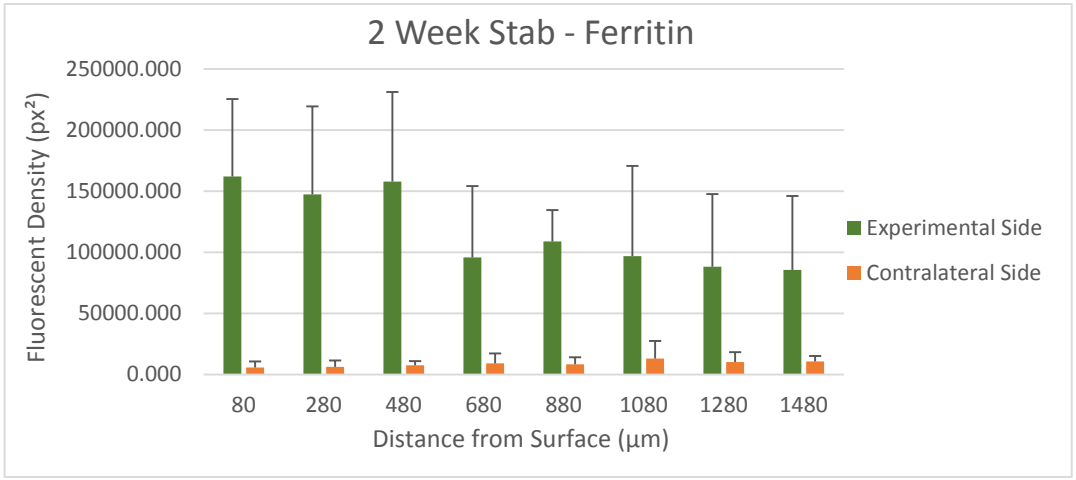

(a)

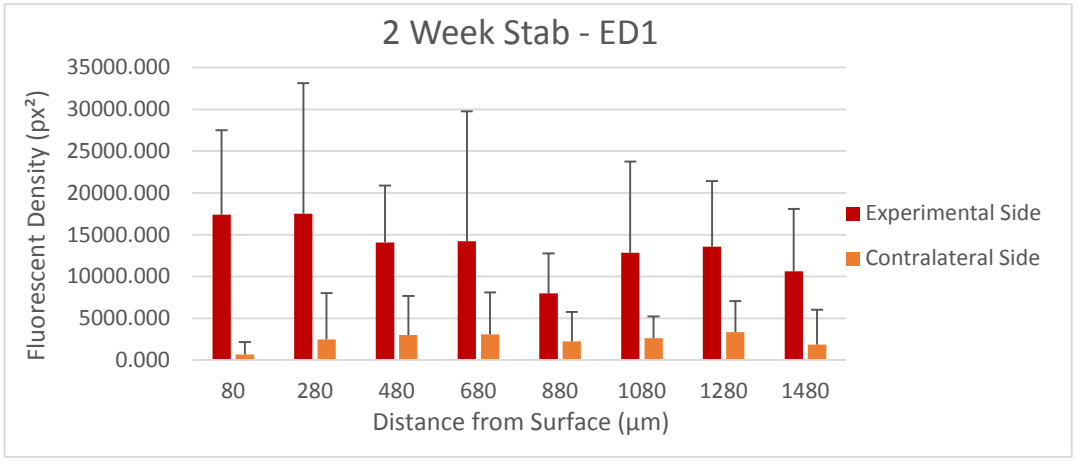

(b)

Figure 4.17: Fluorescent density for each section is out of 4,915,200 px^2. (a) Average fluorescent density for ferritin in two-week stab animals. (b) Average fluorescent density for ED1 in two-week stab animals.

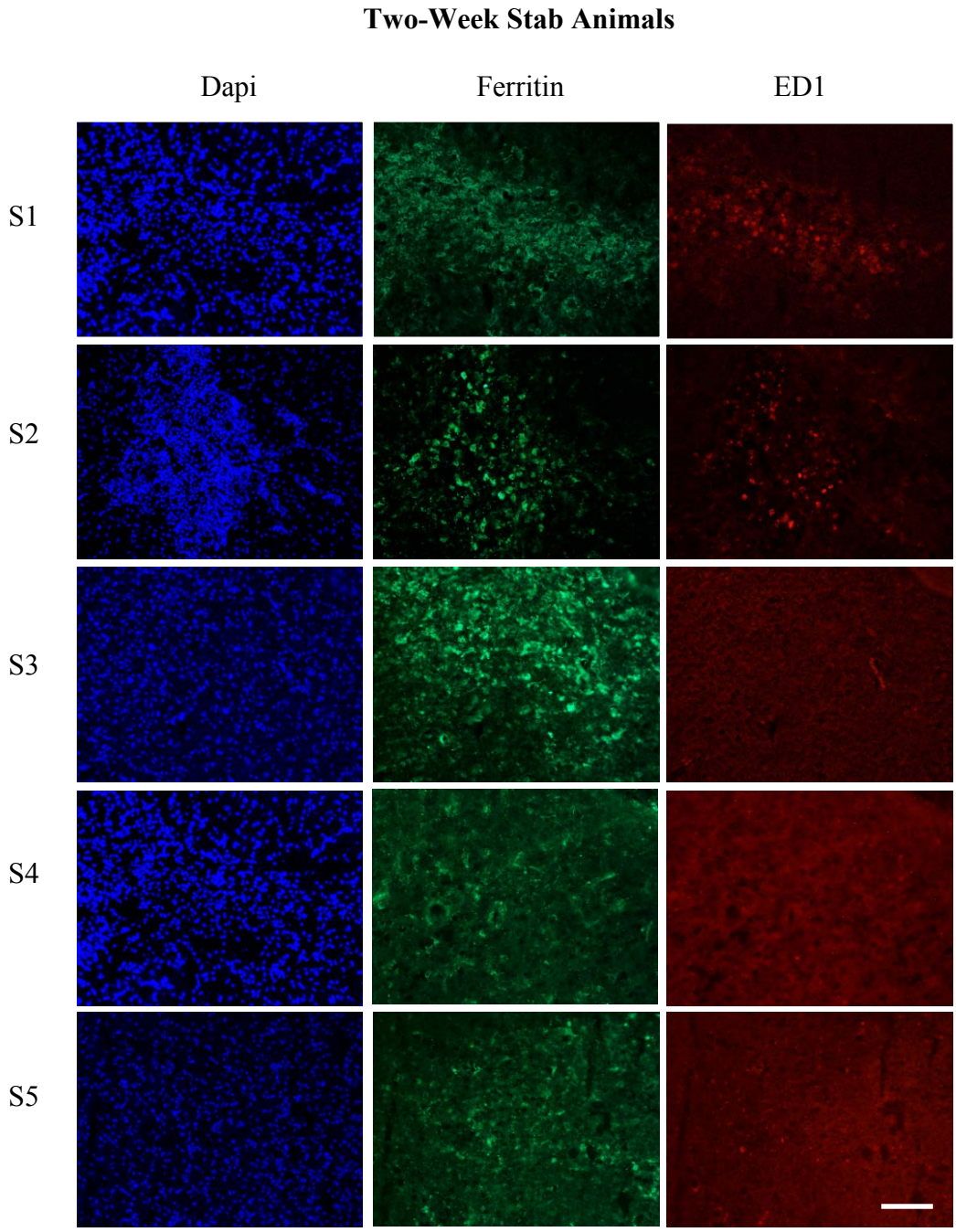

Figure 4.18: Example of acquired fluorescent images for two-week stab animals (S1-5) for Dapi, Ferritin, and ED1. Total fluorescent density of each image is 4,915,200 px^2. Scale bar = 100µm.

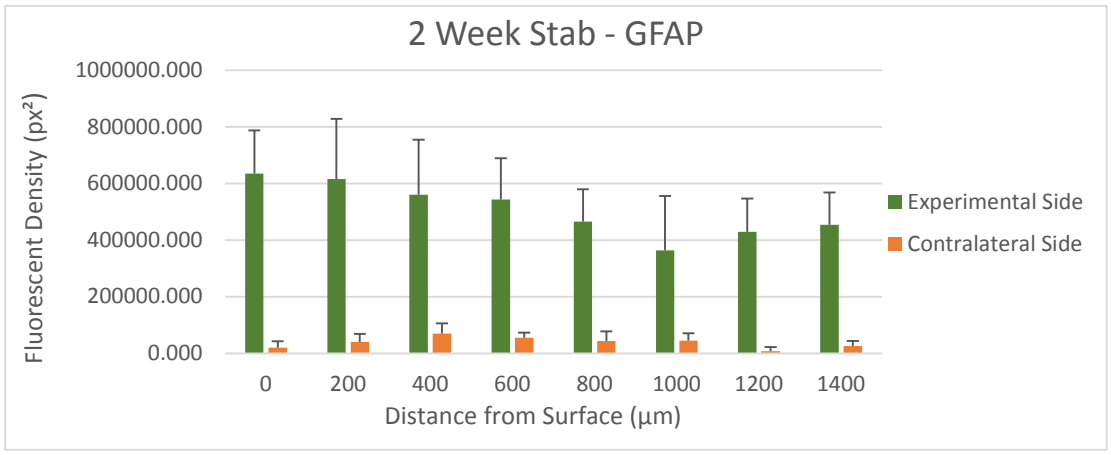

(a)

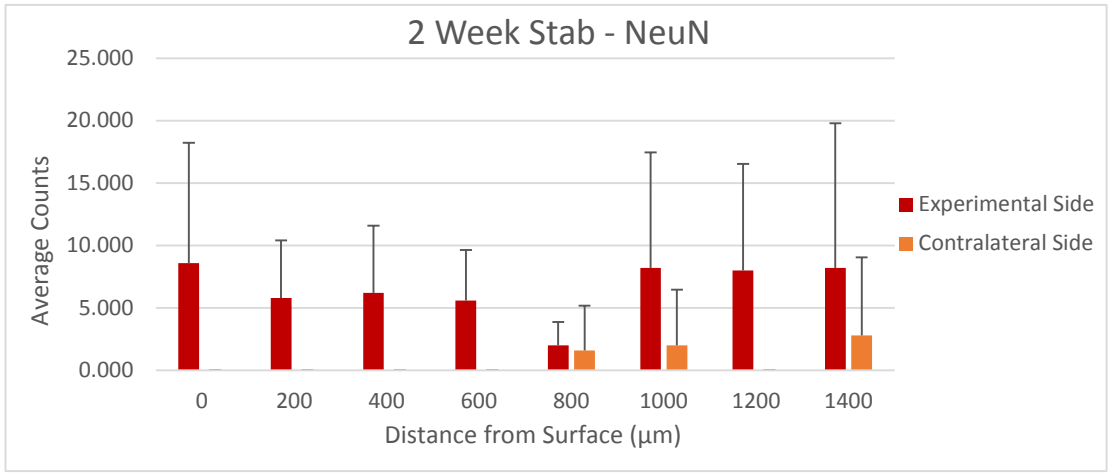

(b)

Figure 4.19: Fluorescent density for each section is out of 4,915,200 px^2. (a) Average fluorescent density for GFAP in two-week stab animals. (b) Average counts of NeuN in two-week stab animals.

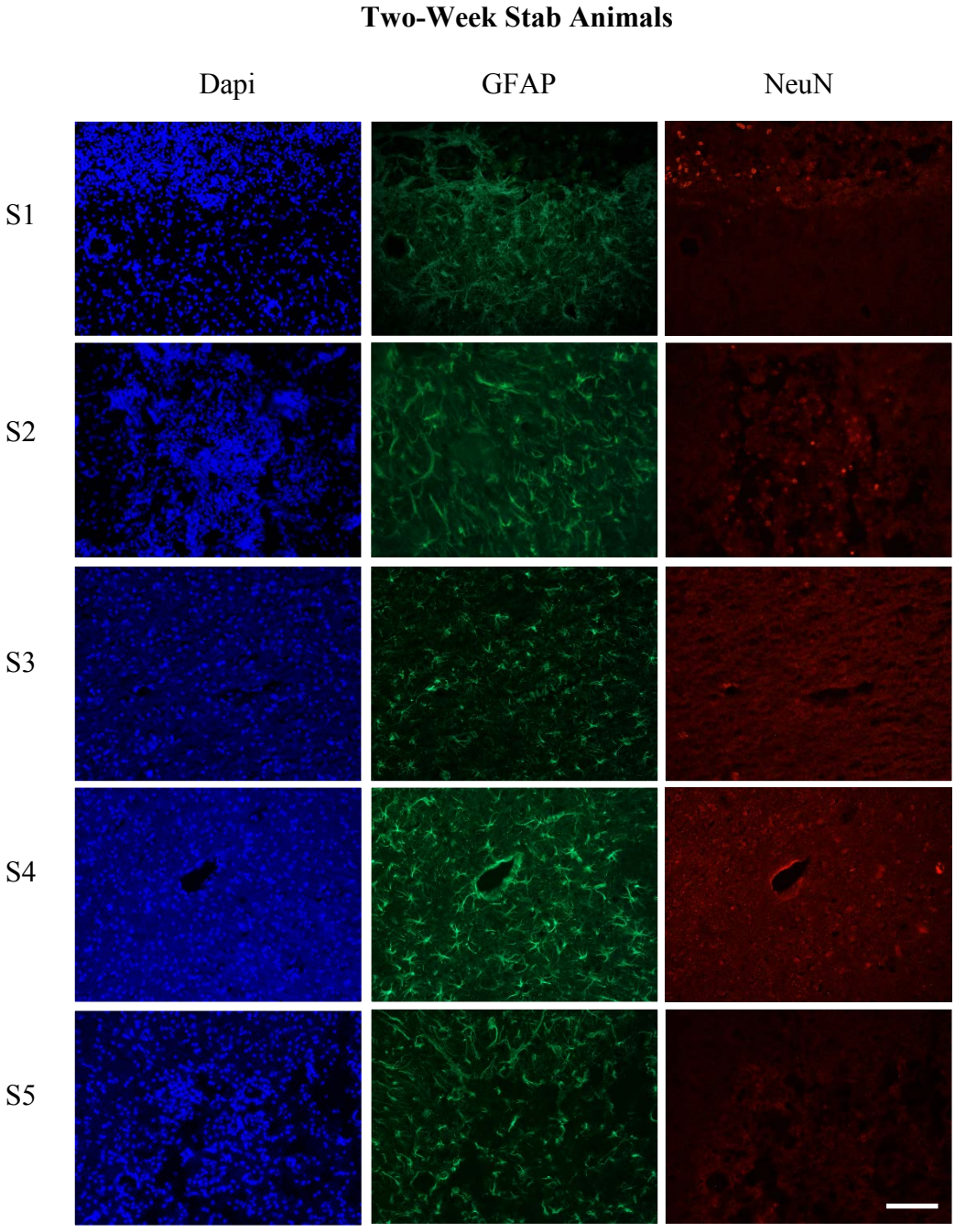

Figure 4.20: Example of acquired fluorescent images for two-week stab animals (S1-5) for Dapi, GFAP, and NeuN. Total fluorescent density of each image is 4,915,200 px^2. Scale bar = 100µm.

4.3.2 Four-Week Stab Animals

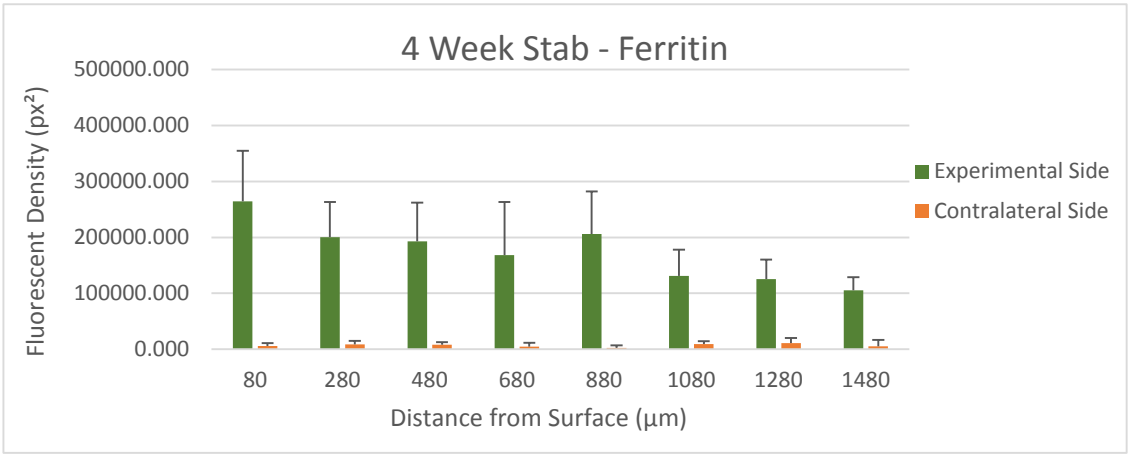

(a)

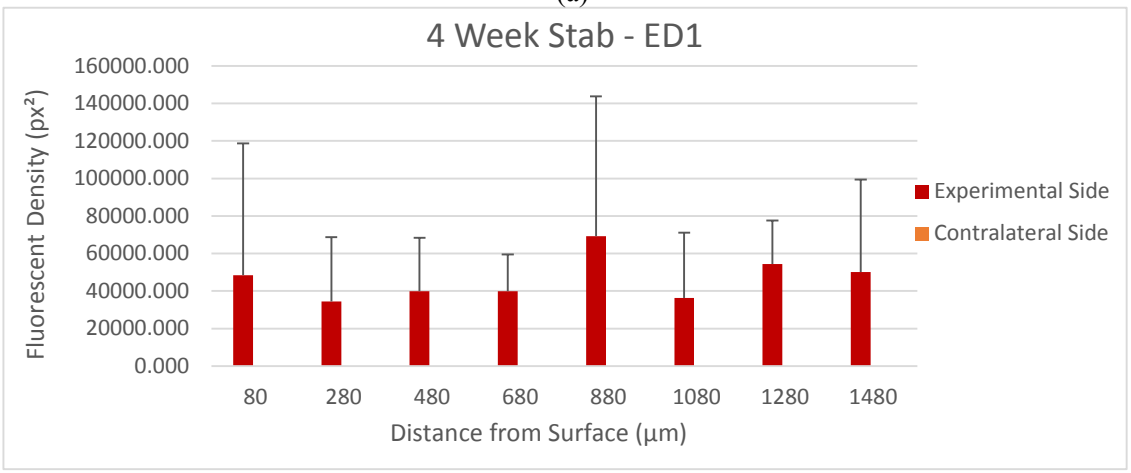

(b)

Figure 4.21: Fluorescent density for each section is out of 4,915,200 px^2. (a) Average fluorescent density for Ferritin in four-week stab animals. (b) Average fluorescent density for ED1 in four-week stab animals.

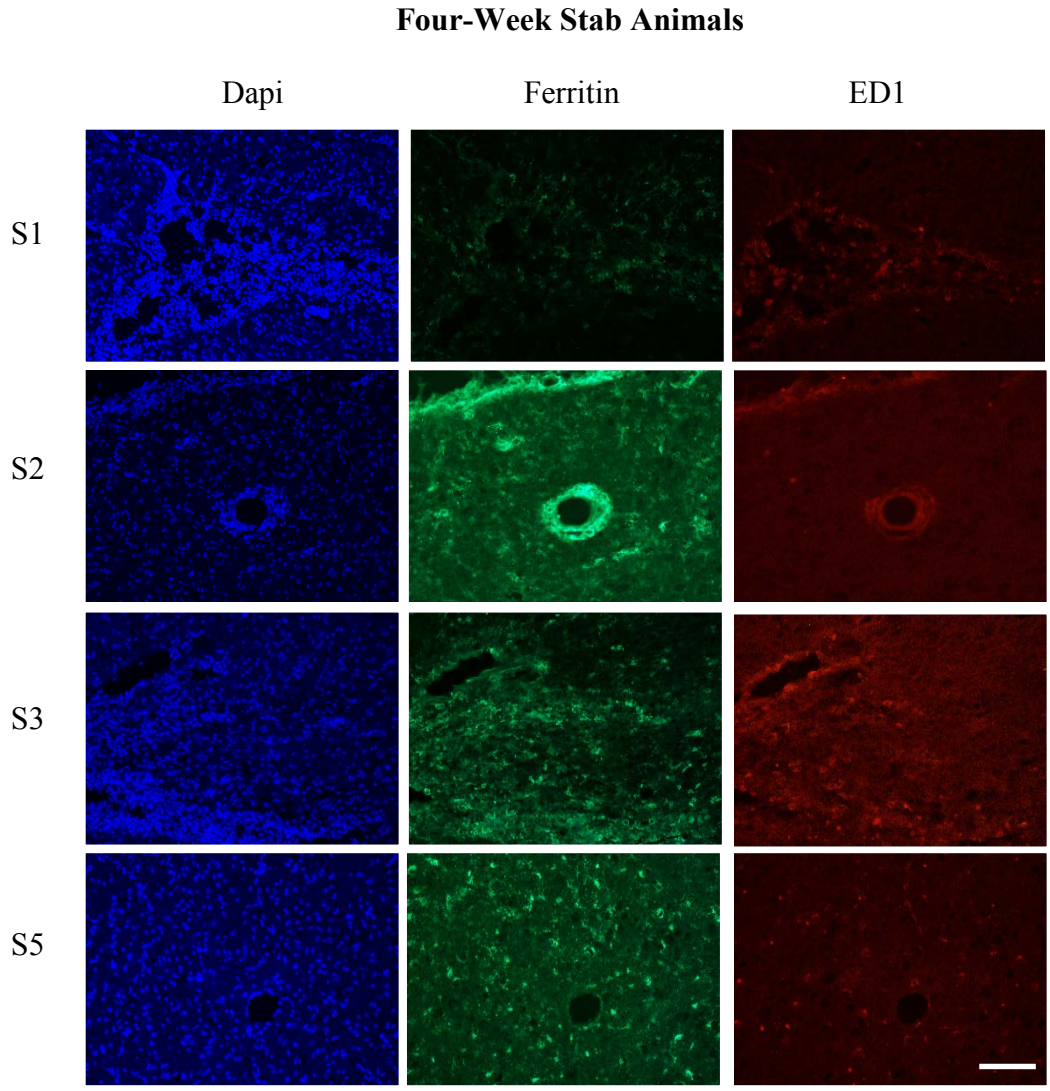

Figure 4.22: Example of acquired fluorescent images for four-week stab animals (S1-3 and S5) for Dapi, Ferritin, and ED1. Animal S4 died of unknown natural causes and no data was able to be collected. Total fluorescent density of each image is 4,915,200 px^2. Scale bar = 100µm.

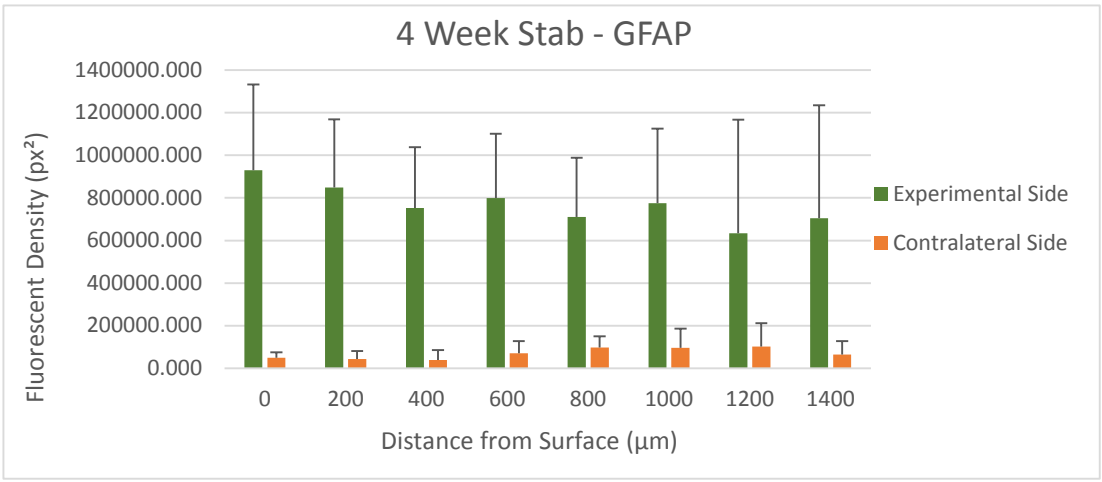

(a)

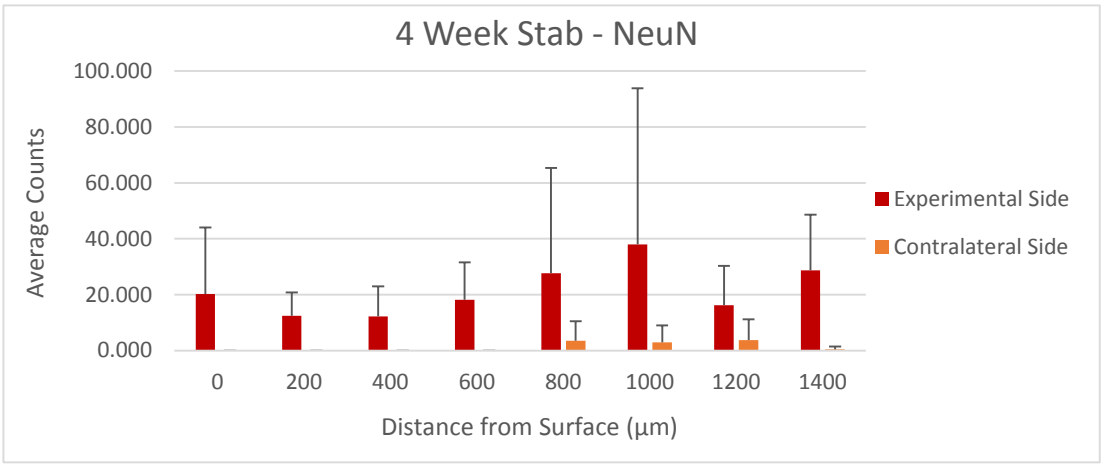

(b)

Figure 4.23: Fluorescent density for each section is out of 4,915,200 px^2. (a) Average fluorescent density for GFAP in four-week stab animals. (b) Average counts of NeuN in four-week stab animals.

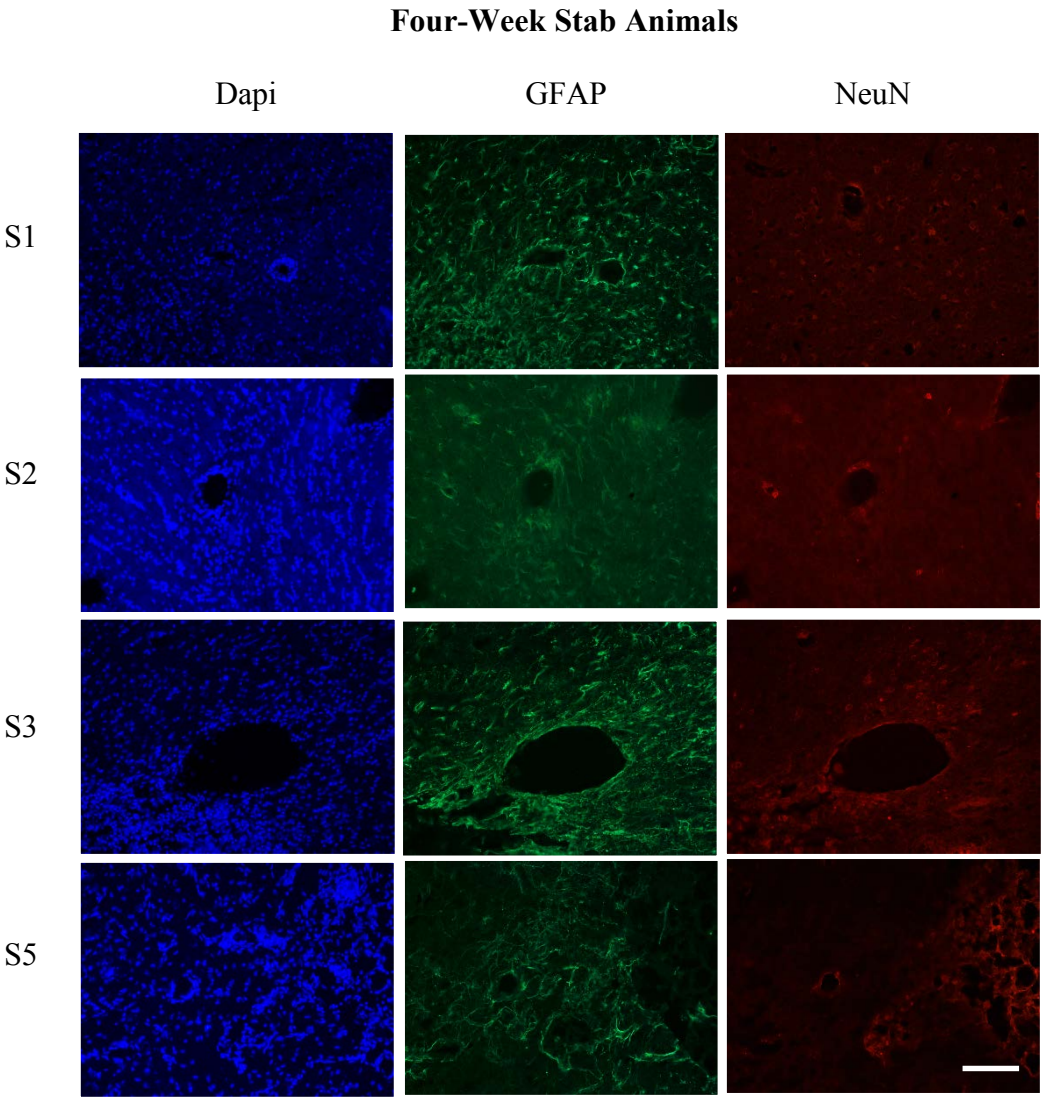

Figure 4.24: Example of acquired fluorescent images for four-week stab animals (S1-3 and S5) for Dapi, GFAP, and NeuN. Animal S4 died of unknown natural causes and no data was able to be collected. Total fluorescent density of each image is 4,915,200 px^2. Scale bar = 100μm.

4.3.3 Four-Week Implant Animals

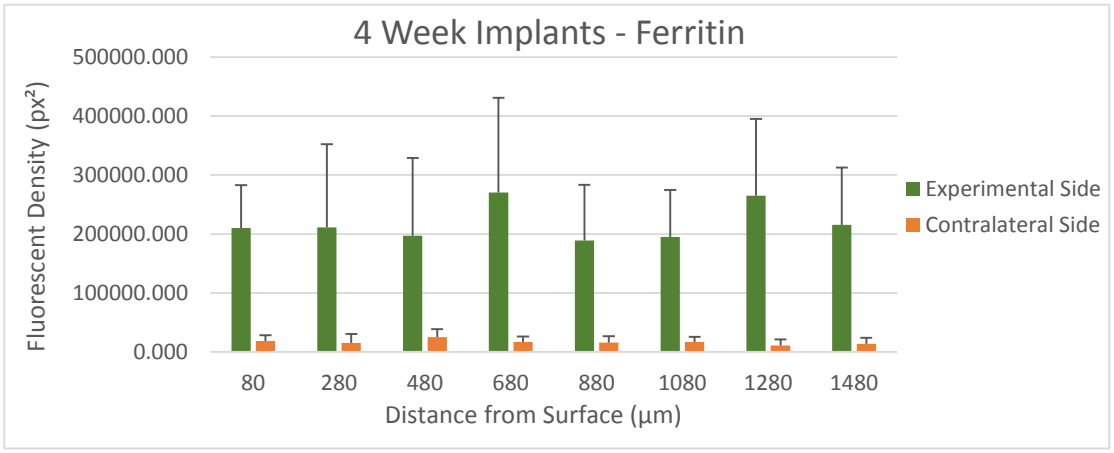

(a)

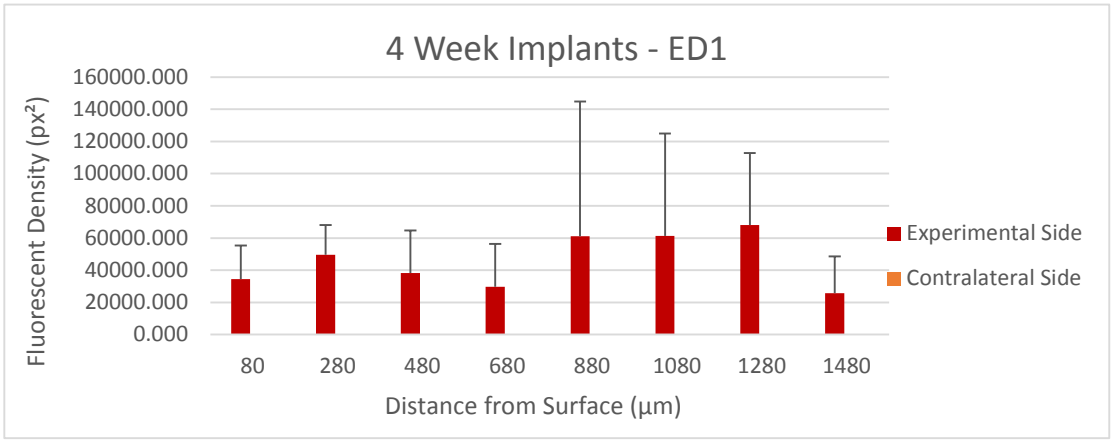

(b)

Figure 4.25: Fluorescent density for each section is out of 4,915,200 px^2. (a) Average fluorescent density for Ferritin in four-week implant animals. (b) Average fluorescent density for ED1 in four-week implant animals.

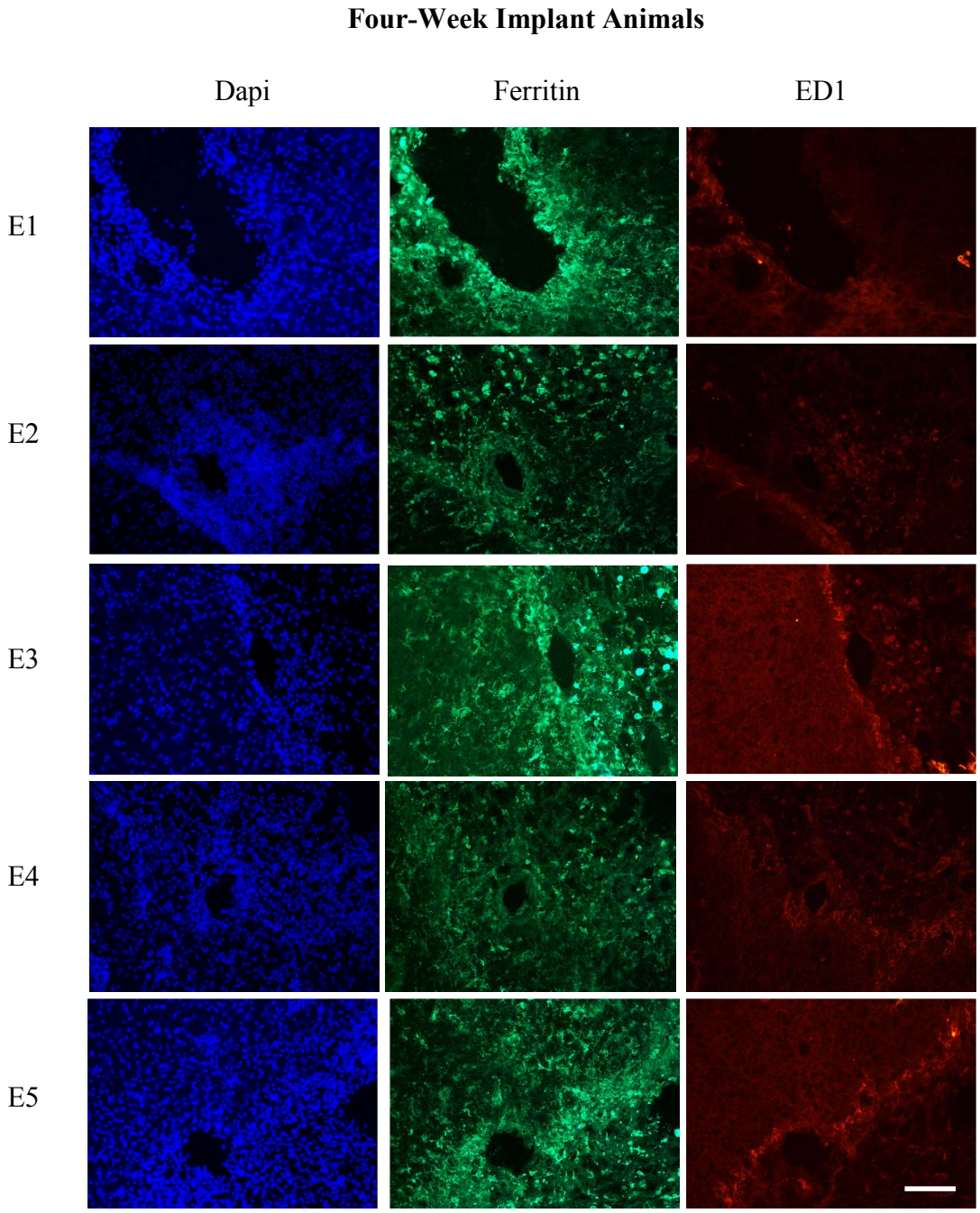

Figure 4.26: Example of acquired fluorescent images for four-week implant animals (E1-5) for Dapi, Ferritin, and ED1. Total fluorescent density of each image is 4,915,200 px^2. Scale bar = 100µm.

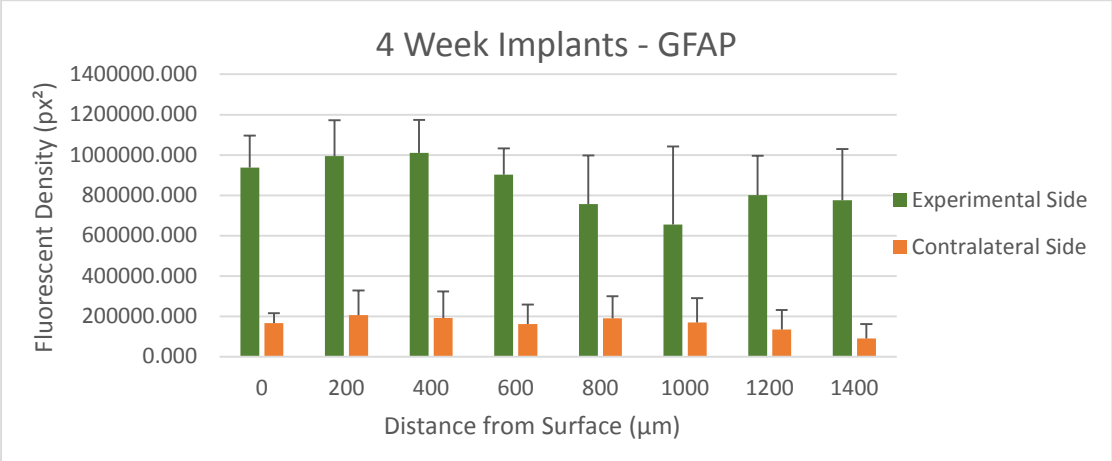

(a)

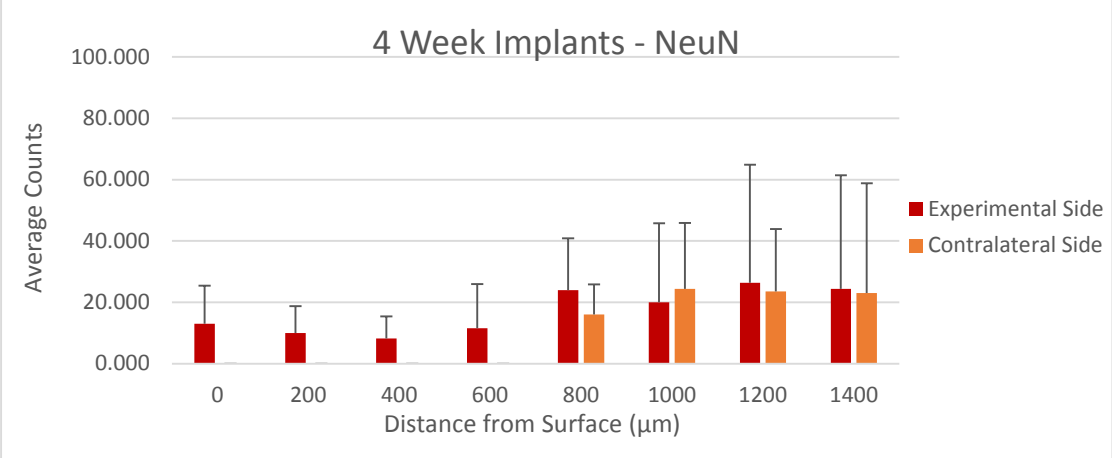

(b)

Figure 4.27: Fluorescent density for each section is out of 4,915,200 px^2. (a) Average fluorescent density for GFAP in four-week implant animals. (b) Average counts of NeuN in four-week implant animals.

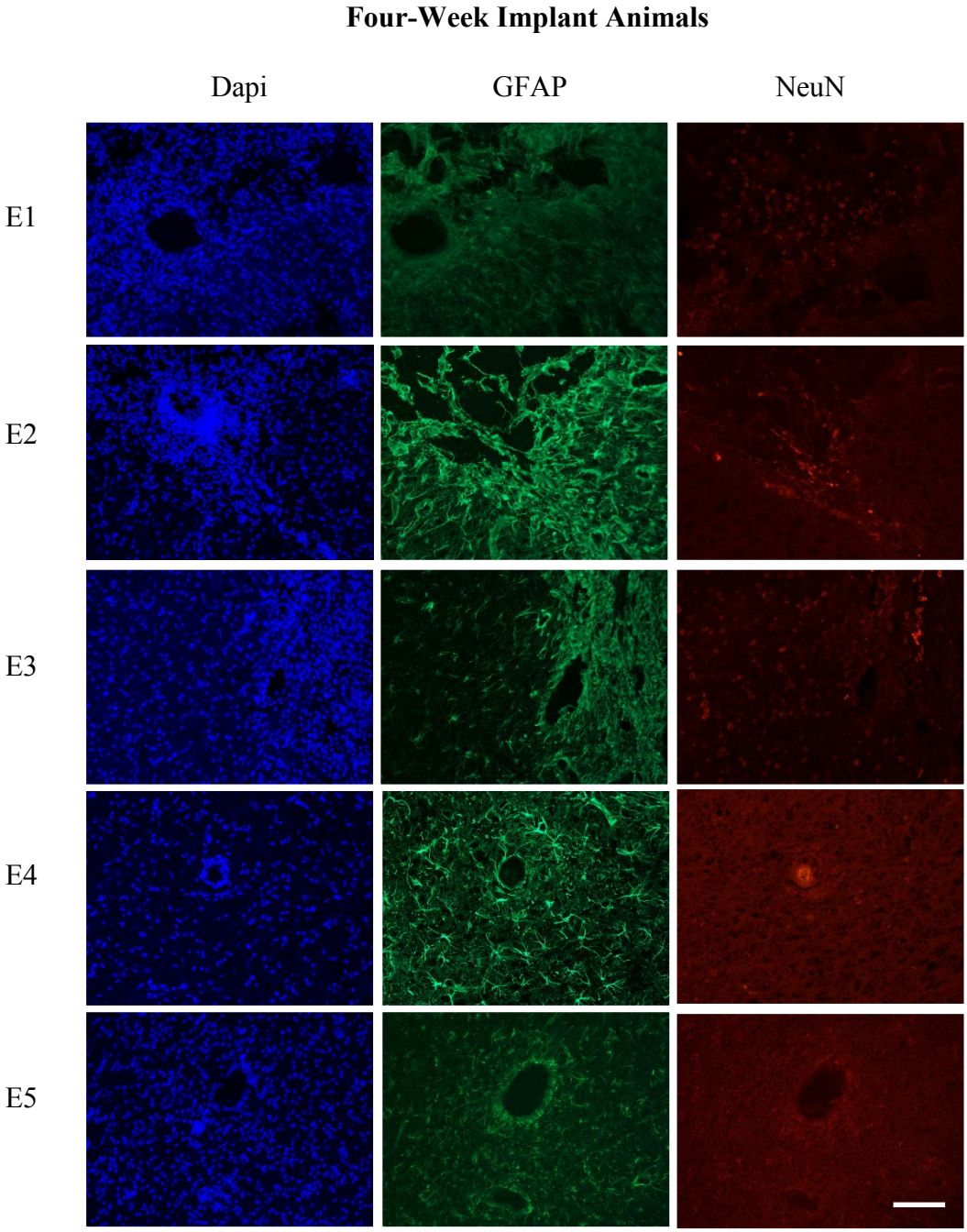

Figure 4.28: Example of acquired fluorescent images for four-week implant animals (E1-5) Dapi, GFAP, and NeuN. Total fluorescent density of each image is 4,915,200 px^2. Scale bar = 100µm.

Chapter 5: Conclusion

In this study, the properties of neuroinflammation and injury were assessed with axonal injury biomarkers, pNF-H and UCHL1, and immunohistochemical markers, ferritin, ED1, GFAP, and NeuN in Utah microelectrode implanted rat brains. These results were used to temporally calculate the immunohistochemical markers of neuroinflammation after acute neural injury.

5.1 Summary

The experimental setup of this thesis allowed the comparison between stabbed and permanently implanted animal cohorts for assessment of their immunohistochemical markers of neural injury after fast insertion of Utah arrays. To our knowledge, no previous studies have explained the neuroinflammation patterns that occur from rapid insertion of Utah microelectrode arrays. As such, the results presented in this thesis show how insertion speed may contribute to the inflammatory response in brain tissue. Immunohistochemical staining provided evidence of reactive astrogliosis and microgliosis, fibrotic tissue formation, and neurodegeneration after an assessment between two- and four-week animal groups. Our results show that higher ED1 expression in longer-term animals is indicative of the ongoing foreign body response leading to activated microglia and macrophages. We also observed greater NeuN counts for longer-time points. On the other hand, ferritin was equally represented between our two timespans, suggesting that vascular disruption and BBB injury occur after the initial insult and, in this case, temporal variation was not a contributing factor. Similarly, GFAP-positive cells had comparable values in two and four week groups since our times points did not fully capture astrocytic encapsulation. Thus, these results suggest that neuroinflammation is an ongoing process leading to activation of

microglia and macrophages, reactive astrocytes, free-iron load, and potential neuron death. We also indicate that the axonal injury biomarkers, pNF-H and UCHL1, can be detected from both sera and CSF, but further experimentation is needed to declare these proteins as reliable markers of neural injury.

Moreover, our results also provided the cross-comparison of the inflammatory response within different depths in the tissue. For instance, we expected greater levels of glial activity and reactivity and free iron closer to the surface of the brain (0-100μm) due to the large and heavy substrate at the top of our electrodes. Our assessments also show signs of increased neuronal yield closer to the electrode tip (800-1480μm). Based on the data gathered, we note that our main contributing factor to this experiment is the rapid insertion of the arrays. Thus, herein we note that the initial insult caused by fast insertion of Utah microelectrodes may be an important contributor of neuroinflammation.

5.2 Limitations

To obtain a more global picture of biomarker expression and cellular activation, longer time points of implantation should be considered. Longer-term implants could reduce the probabilities of errors and increase the possibilities of observing the entire injury, from high to low indications of neuroinflammation through measurements of increasing and decreasing pNF-H, UCHL1, and immunohistochemical marker expression. Performing this set of experiments alongside a microelectrode with slow insertion could also provide more detail about the effects of rapid insertion damage with these arrays.

REFERENCES

Abbas, A. K., Lichtman, A. H., & Pillai, S. (2003). *Cellular and molecular immunology* (8th ed.). Philadelphia: Saunders.

Anderson, J. M., Rodriguez, A., & Chang, D. T. (2008). Foreign body reaction to biomaterials. *Seminars in Immunology, 20*(2), 86-100.

Anderson, K. J., Scheff, S. W., Miller, K. M., Roberts, K. N., Gilmer, L. K., Yang, C., & Shaw, G. (2008). The phosphorylated axonal form of the neurofilament subunit NF-H (pNF-H) as a blood biomarker of traumatic brain injury. *Journal of Neurotrauma, 25*(9), 1079-1085.

Bear, M. F., Connors, B. W., & Paradiso, M. A. (2007). *Neuroscience: exploring the brain*. Philadelphia, PA: Lippincott Williams & Wilkins.

Biran, R., Martin, D. C., & Tresco, P. A. (2005). Neuronal cell loss accompanies the brain tissue response to chronically implanted silicon microelectrode arrays. *Experimental Neurology, 195*(1), 115-126.

Block, M. L., Zecca, L., & Hong, J. (2007). Microglia-mediated neurotoxicity: uncovering the molecular mechanisms. *Nature Reviews Neuroscience, 8*(1), 57-69.

Boylan, K., Yang, C., Crook, J., Overstreet, K., Heckman, M., Wang, Y., . . . Shaw, G. (2009). Immunoreactivity of the phosphorylated axonal neurofilament H subunit (pNF-H) in blood of ALS model rodents and ALS patients: evaluation of blood pNF-H as a potential ALS biomarker. *Journal of Neurochemistry, 111*(5), 1182-1191.

Dahlke, C., Saberi, D., Ott, B., Brand-Saberi, B., Schmitt-John, T., & Theiss, C. (2015). Inflammation and neuronal death in the motor cortex of the wobbler mouse, an ALS animal model. *Journal of Neuroinflammation, 12*(1), 1-11.

Dash, P. K., Zhao, J., Hergenroeder, G., & Moore, A. N. (2010). Biomarkers for the diagnosis, prognosis, and evaluation of treatment efficacy for traumatic brain injury. *The Journal of the American Society for Experimental NeuroTherapeutics, 7*(1), 100-114.

Doran, J. F., Jackson, P., Kynoch, P. A., & Thompson, R. J. (1983). Isolation of PGP 9.5, a new human neurone-specific protein detected by high-resolution two-dimensional electrophoresis. *Journal of Neurochemistry, 40*(6), 1542-1547.

Fernández, E., Greger, B., House, P. A., Aranda, I., Botella, C., Albisua, J., . . . Normann, R. A. (2014). Acute human brain responses to intracortical microelectrode arrays: Challenges and future prospects. *Frontiers in Neuroengineering, 7*.

Fleming, J. C., Norenberg, M. D., Ramsay, D. A., Dekaban, G. A., Marcillo, A. E., Saenz, A. D., Weaver, L. C. (2006). The cellular inflammatory response in human spinal cords after injury. *Brain, 129*(12), 3249-3269.

Freire, M. M., Morya, E., Faber, J., Santos, J. R., Guimaraes, J. S., Lemos, N. A., . . . Nicolelis, M. A. (2011). Comprehensive analysis of tissue preservation and recording quality from chronic multielectrode implants. *PLoS ONE, 6*(11).

Geddes, L. A., & Roeder, R. (2003). Criteria for the selection of materials for implanted electrodes. *Annals of Biomedical Engineering, 31*(7), 879-890.

Ghonemi, M. O., Rabah, A. A., Saber, H. M., & Radwan, W. (2013). Role of Phosphorylated Neurofilament H as a diagnostic and prognostic marker in traumatic brain injury. *The Egyptian Journal of Critical Care Medicine, 1*(3), 139-144.

Graeber, M. B., & Streit, W. J. (2009). Microglia: biology and pathology. *Acta Neuropathologica, 119*(1), 89-105.

Gresle, M. M., Shaw, G., Jarrott, B., Alexandrou, E. N., Friedhuber, A., Kilpatrick, T. J., & Butzkueven, H. (2008). Validation of a novel biomarker for acute axonal injury in experimental autoimmune encephalomyelitis. *Journal of Neuroscience Research, 86*(16), 3548-3555.

Gusel'nikova, V. V., & Korzhevskiy, D. E. (2015). NeuN As a neuronal nuclear antigen and neuron differentiation marker. *Acta Naturae*, *7*(2), 42-47.

Guy, J., Shaw, G., Ross-Cisneros, F. N., Quiros, P., Salomao, S. R., Berezovsky, A., . . . Sadun, A. A. (2008). Phosphorylated neurofilament heavy chain is a marker of neurodegeneration in Leber hereditary optic neuropathy (LHON). *Molecular Vision, 14*, 2443-2450.

Hayakawa, K., Okazaki, R., Ishii, K., Ueno, T., Izawa, N., Tanaka, Y., . . . Ogata, T. (2012). Phosphorylated neurofilament subunit NF-H as a biomarker for evaluating the severity of spinal cord injury patients, a pilot study. *Spinal Cord, 50*(7), 493-496.

Hoffman, G. E., Le, W. W., & Sita, L. V. (2008). The importance of titrating antibodies for immunocytochemical methods. *Current Protocols in Neuroscience, 2-12*, 1-26.

Hu, Y., He, S., Wang, X., Duan, Q., Khatoon, S., Iqbal, K., . . . Wang, J. (2002). Elevated levels of phosphorylated neurofilament proteins in cerebrospinal fluid of Alzheimer disease patients. *Neuroscience Letters, 320*(3), 156-160.

Khan, A. S., & Michael, A. C. (2003). Invasive consequences of using micro-electrodes and microdialysis probes in the brain. *Trends in Analytical Chemistry, 22*(8), 503-508.

Kozai, T. D., Catt, K., Li, X., Gugel, Z. V., Olafsson, V. T., Vazquez, A. L., & Cui, X. T. (2015). Mechanical failure modes of chronically implanted planar silicon-based neural probes for laminar recording. *Biomaterials, 37*, 25-39.

Lacour, S. P., Benmerah, S., Tarte, E., Fitzgerald, J., Serra, J., Mcmahon, S., . . . Morrison, B. (2010). Flexible and stretchable micro-electrodes for in vitro and in vivo neural interfaces. *Medical, Biological Engineering and Computing, 48*(10), 945-954.

Lee, V. M., Otvos, L., Carden, M. J., Hollosi, M., Dietzschold, B., & Lazzarini, R. A. (1988). Identification of the major multiphosphorylation site in mammalian neurofilaments. *Proceedings of the National Academy of Sciences, 85*(6), 1998-2002.

Lewis, S. B., Wolper, R., Chi, Y., Miralia, L., Wang, Y., Yang, C., & Shaw, G. (2010). Identification and preliminary characterization of ubiquitin C terminal hydrolase 1 (UCHL1) as a biomarker of neuronal loss in aneurysmal subarachnoid hemorrhage. *Journal of Neuroscience Research, 88*, 1475-1484.

Lewis, S. B., Wolper, R. A., Miralia, L., Yang, C., & Shaw, G. (2008). Detection of phosphorylated NF-H in the cerebrospinal fluid and blood of aneurysmal subarachnoid hemorrhage patients. *Journal of Cerebral Blood Flow & Metabolism, 28*(6), 1261-1271.

Liu, Y., Fallon, L., Lashuel, H. A., Liu, Z., & Lansbury, P. T. (2002). The UCH-L1 gene encodes two opposing enzymatic activities that affect α-synuclein degradation and Parkinson's disease susceptibility. *Cell, 111*(2), 209-218.

Lodish, H., & Zipursky, S. L. (200). Overview of neuron structure and function. In A. Berk (Ed.), *Molecular Cell Biology* (4th ed.). New York, NY: W. H. Freeman.

Lv, R., Mao, N., Wu, J., Lu, C., Ding, M., Gu, X., . . . Shi, Z. (2015). Neuroprotective effect of allicin in a rat model of acute spinal cord injury. *Life Sciences, 143*, 114-123.

Matsushige, T., Ichiyama, T., Anlar, B., Tohyama, J., Nomura, K., Yamashita, Y., & Furukawa, S. (2008). CSF neurofilament and soluble TNF receptor 1 levels in subacute sclerosing panencephalitis. *Journal of Neuroimmunology, 205*(1-2), 155-159.

Maynard, E. M., Nordhausen, C. T., & Normann, R. A. (1997). The Utah Intracortical Electrode Array: A recording structure for potential brain-computer interfaces. *Electroencephalography and Clinical Neurophysiology, 102*(3), 228-239.

Mccombe, P., Pfluger, C., Singh, P., Lim, C., Airey, C., & Henderson, R. (2015). Serial measurements of phosphorylated neurofilament-heavy in the serum of subjects with amyotrophic lateral sclerosis. *Journal of the Neurological Sciences, 353*(1-2), 122-129.

Mcconnell, G. C., Rees, H. D., Levey, A. I., Gutekunst, C., Gross, R. E., & Bellamkonda, R. V. (2009). Implanted neural electrodes cause chronic, local inflammation that is correlated with local neurodegeneration. *Journal of Neural Engineering, 6*(5), 056003-0560015.

Mccreery, D. B., Yuen, T. G., Agnew, W. F., & Bullara, L. A. (1997). A characterization of the effects on neuronal excitability due to prolonged microstimulation with chronically implanted microelectrodes. *IEEE Transactions on Biomedical Engineering, 44*(10), 931-939.

Mehdiratta, M., Kumar, S., Hackney, D., Schlaug, G., & Selim, M. (2008). Association between serum ferritin level and perihematoma edema volume in patients with spontaneous intracerebral hemorrhage. *Stroke, 39*(4), 1165-1170.

Mondello, S., Muller, U., Jeromin, A., Streeter, J., Hayes, R. L., & Wang, K. K. (2011). Blood-based diagnostics of traumatic brain injuries. *Expert Review of Molecular Diagnostics, 11*(1), 65-78.

Muszynski, J. A., Thakkar, R., & Hall, M. W. (2016). Inflammation and innate immune function in critical illness. *Current Opinion in Pediatrics, 28*(3), 267-273.

Nicolelis, M. A., & Ribeiro, S. (2002). Multielectrode recordings: The next steps. *Current Opinion in Neurobiology, 12*(5), 602-606.

Nordhausen, C. T., Rousche, P. J., & Normann, R. A. (1994). Optimizing recording capabilities of the Utah intracortical electrode array. *Brain Research, 637*(1-2), 27-36.

Ohya, J., Chikuda, H., Kato, S., Hayakawa, K., Oka, H., Takeshita, K., . . . Ogata, T. (2015). Elevated levels of phosphorylated neurofilament heavy subunit in the cerebrospinal fluid of patients with lumbar spinal stenosis: preliminary findings. *The Spine Journal, 15*(7), 1587-1592.

Pant, H. C. (1988). Dephosphorylation of neurofilament proteins enhances their susceptibility to degradation by calpain. *Biochemical Journal, 256*(2), 665-668.

Papa, L., Akinyi, L., Liu, M. C., Pineda, J. A., Tepas, J. J., Oli, M. W., . . . Wang, K. K. (2010). Ubiquitin C-terminal hydrolase is a novel biomarker in humans for severe traumatic brain injury*. *Critical Care Medicine, 38*(1), 138-144.

Petzold, A. (2005). Neurofilament phosphoforms: Surrogate markers for axonal injury, degeneration and loss. *Journal of the Neurological Sciences, 233*(1-2), 183-198.

Petzold, A., & Shaw, G. (2007). Comparison of two ELISA methods for measuring levels of the phosphorylated neurofilament heavy chain. *Journal of Immunological Methods, 319*(1-2), 34-40.

Polikov, V. S., Tresco, P. A., & Reichert, W. M. (2005). Response of brain tissue to chronically implanted neural electrodes. *Journal of Neuroscience Methods, 148*(1), 1-18.

Prasad, A., Sankar, V., Dyer, A. T., Knott, E., Xue, Q., Nishida, T., . . . Sanchez, J. C. (2011). Coupling biotic and abiotic metrics to create a testbed for predicting neural electrode performance. *2011 Annual International Conference of the IEEE Engineering in Medicine and Biology Society,* 3020-3023.

Prasad, A., Xue, Q., Sankar, V., Nishida, T., Shaw, G., Streit, W. J., & Sanchez, J. C. (2012). Comprehensive characterization and failure modes of tungsten microwire arrays in chronic neural implants. *Journal of Neural Engineering, 9*(5), 056015-056036.

Prasad, A., & Sanchez, J. C. (2012). Quantifying long-term microelectrode array functionality using chronic in vivo impedance testing. *Journal of Neural Engineering, 9*(2), 026028-026030.

Prasad, A., Xue, Q., Dieme, R., Sankar, V., Mayrand, R. C., Nishida, T., . . . Sanchez, J. C. (2014). Abiotic-biotic characterization of Pt/Ir microelectrode arrays in chronic implants. *Frontiers in Neuroengineering, 7*(2), 1-15.

Ramos-Vara, J. A., & Miller, M. A. (2013). When tissue antigens and antibodies get along: revisiting the technical aspects of immunohistochemistry--the red, brown, and blue technique. *Veterinary Pathology, 51*(1), 42-87.

Rock, K. L., & Kono, H. (2008). The inflammatory response to cell death. *Annual Review of Pathology: Mechanisms of Disease, 3*(1), 99-126.

Rousche, P. J., & Normann, R. A. (1992). A method for pneumatically inserting an array of penetrating electrodes into cortical tissue. *Annals of Biomedical Engineering, 20*(4), 413-422.

Rousche, P. J., & Normann, R. A. (1998). Chronic recording capability of the Utah intracortical electrode array in cat sensory cortex. *Journal of Neuroscience Methods, 82*(1), 1-15.

Shaw, G., Yang, C., Ellis, R., Anderson, K., Mickle, J. P., Scheff, S., . . . Howland, D. R. (2005). Hyperphosphorylated neurofilament NF-H is a serum biomarker of axonal injury. *Biochemical and Biophysical Research Communications, 336*(4), 1268-1277.

Siman, R., Roberts, V. L., Mcneil, E., Dang, A., Bavaria, J. E., Ramchandren, S., & Mcgarvey, M. (2008). Biomarker evidence for mild central nervous system injury after surgically-induced circulation arrest. *Brain Research, 1213*, 1-11.

Singh, P., Yan, J., Hull, R., Read, S., O'sullivan, J., Henderson, R., . . . Mccombe, P. (2011). Levels of phosphorylated axonal neurofilament subunit H (pNfH) are increased in acute ischemic stroke. *Journal of the Neurological Sciences, 304*(1-2), 117-121.

Spataro, L., Dilgen, J., Retterer, S., Spence, A., Isaacson, M., Turner, J., & Shain, W. (2005). Dexamethasone treatment reduces astroglia responses to inserted neuroprosthetic devices in rat neocortex. *Experimental Neurology, 194*(2), 289-300.

Sternberger, L. A., & Sternberger, N. H. (1983). Monoclonal antibodies distinguish phosphorylated and nonphosphorylated forms of neurofilaments in situ. *Proceedings of the National Academy of Sciences, 80*(19), 6126-6130.

Stys, P. K. (2005). General mechanisms of axonal damage and its prevention. *Journal of the Neurological Sciences, 233*(1-2), 3-13.

Szarowski, D., Andersen, M., Retterer, S., Spence, A., Isaacson, M., Craighead, H., . . . Shain, W. (2003). Brain responses to micro-machined silicon devices. *Brain Research, 983*(1-2), 23-35.

Turner, J. N., Shain, W., Szarowski, D. H., Andersen, M., Martins, S., Isaacson, M., & Craighead, H. (1999). Cerebral Astrocyte Response to Micromachined Silicon Implants. Experimental Neurology, 156(1), 33-49.

Ünal-Çevik, I., Kılınç, M., Gürsoy-Özdemir, Y., Gurer, G., & Dalkara, T. (2004). Loss of NeuN immunoreactivity after cerebral ischemia does not indicate neuronal cell loss: A cautionary note. *Brain Research, 1015*(1-2), 169-174.

Vilhardt, F. (2005). Microglia: phagocyte and glia cell. *The International Journal of Biochemistry and Cell Biology, 37*(1), 17-21.

Wilkinson, K., Lee, K., Deshpande, S., Duerksen-Hughes, P., Boss, J., & Pohl, J. (1989). The neuron-specific protein PGP 9.5 is a ubiquitin carboxyl-terminal hydrolase. *Science, 246*(4930), 670-673.

Williams, J. C., Rennaker, R. L., & Kipke, D. R. (1999). Long-term neural recording characteristics of wire microelectrode arrays implanted in cerebral cortex. *Brain Research Protocols, 4*(3), 303-313.

Winslow, B. D., & Tresco, P. A. (2010). Quantitative analysis of the tissue response to chronically implanted microwire electrodes in rat cortex. *Biomaterials, 31*(7), 1558-1567.

Yiu, G., & He, Z. (2006). Glial inhibition of CNS axon regeneration. *Nature Reviews Neuroscience, 7*(8), 617-627.

Zhang, S., Chen, X., Gu, C., Zhang, Y., Xu, J., Bian, Z., . . . Gu, N. (2008). The effect of iron oxide magnetic nanoparticles on smooth muscle cells. *Nanoscale Research Letters, 4*(1), 70-77.

Žurek, J., Bartlová, L., & Fedora, M. (2011). Hyperphosphorylated neurofilament NF-H as a predictor of mortality after brain injury in children. *Brain Injury, 25*(2), 221-226.